

EMISSION-LINE SPECTRA OF S VII–S XIV IN THE 20–75 Å WAVELENGTH REGION

J. K. LEPSON

Space Sciences Laboratory, 7 Gauss Way, University of California, Berkeley, CA 94720-7450; lepson@ssl.berkeley.edu

P. BEIERSDORFER

Department of Physics and Advanced Technology, Lawrence Livermore National Laboratory,
Livermore, CA 94550; beiersdorfer@llnl.gov

E. BEHAR

Physics Department, Technion-Israel Institute of Technology, Haifa 32000, Israel; behar@physics.technion.ac.il

AND

S. M. KAHN

Physics Department, Stanford University, Stanford, CA 94305; skahn@slac.stanford.edu

Received 2004 July 27; accepted 2005 February 24

ABSTRACT

As part of a larger project to complete a comprehensive catalog of astrophysically relevant emission lines in support of new-generation X-ray observatories using the Lawrence Livermore electron beam ion traps EBIT-I and EBIT-II, we present observations of sulfur lines in the soft X-ray and extreme-ultraviolet regions. Our database includes wavelength measurements with standard errors, relative intensities, and line assignments for 127 transitions of S VII through S XIV between 20 and 75 Å. The experimental data are complemented with a full set of calculations using the Hebrew University Lawrence Livermore Atomic Code (HULLAC). A comparison of the laboratory data with *Chandra* measurements of Procyon allows us to identify S VII–S XI lines.

Subject headings: line: identification — methods: analytical — methods: laboratory — stars: coronae — stars: individual (Procyon)

1. INTRODUCTION

Satellite observations in the extreme-ultraviolet (EUV) region provide unique and valuable diagnostic opportunities for astronomers and astrophysicists. The EUV spectral region, which at the short-wavelength side overlaps with the soft X-ray region, contains a wealth of emission lines that can be used for determining plasma properties and elemental abundances over a wide temperature range. The region between 20 and 80 Å has received scant attention, however, even in solar measurements. Previous observations by the *Extreme Ultraviolet Explorer* stopped at 70 Å, while crystal spectrometers on board various missions covered the regions below 20 Å. An exception was the Diffuse X-Ray Spectrometer (DXS), which explored the 44–84 Å region, albeit with a rather low resolution of ~ 1 Å, during the space shuttle *Endeavour* mission STS-54 in 1993. The lack of reliable wavelength and emission data in this region became apparent when trying to analyze the spectra (Sanders et al. 2001). Because this region has been virtually unstudied, even in the laboratory, the relevant databases are essentially empty. Observations in the soft X-ray region by the *Chandra X-Ray Observatory* and *XMM-Newton* are now providing high-resolution measurements, which have far outpaced the databases. There are many more lines in these spectra than can be currently identified, as is graphically illustrated by *Chandra* spectra of Capella (Brinkman et al. 2000) and Procyon (Raassen et al. 2002).

Line lists for the L-shell emission of all elements aside from iron are highly deficient. (For iron, see Brown et al. 2002 and Behar et al. 2001) In the case of sulfur, for example, the MEKAL database (Mewe et al. 1995a) includes 47 lines for S VII through S XIV between 20 and 75 Å. The CHIANTI database (ver. 3.0; Dere et al. 1997, 2001) includes 13 lines of S XIV but only nine lines for the other charge states of sulfur, for a total of 22 lines. However, long-term exposures of stellar coronae have shown a

wealth of weak lines. These weak lines raise the “background” level for the brighter, known lines and add uncertainty to their interpretation. Moreover, they obscure the true thermal background level, requiring various assumptions to fit the background level, for example, a hotter plasma temperature, abundances reduced from the solar value, or changes in assumed absorption. (Beiersdorfer et al. 1999b; Schmitt et al. 1996; Mewe et al. 1995b). Contributions to these unidentified lines may come from magnesium, sulfur, argon, calcium, iron, and nickel. Identification of as many ions as possible of a given element provides a measurement of the emission measure (EM) distribution shape, which is independent of assumptions about the chemical composition. In fact, the only reliable method to disentangle the temperature and the chemical structures and to obtain robust, model-independent abundance values is to compare the EM distribution derived from many ions of different elements. The line emissions of L-shell ions are a crucial addition to the K-shell lines regularly observed in astrophysical X-ray spectra, but the uncertainties associated with the wavelengths and intensities of L-shell lines greatly impede our efforts to fully understand astrophysical X-ray sources. Calculations are helpful to predict emission from these elements. A major problem is that the accuracy of the calculated wavelengths is limited, as the structure of the intermediate ionization stages of all high-Z ions of astrophysical interest are significantly affected by electron-electron interactions, and these ionization stages must be calculated in intermediate coupling. Wavelength errors of a percent are not uncommon. No ab initio code can consistently calculate wavelengths to better than a few tenths of a percent for mid-Z L-shell or M-shell ions, albeit some progress has been made in accurate wavelength calculations by applying many-body perturbation theory to L-shell ions, producing significantly better agreement with laboratory data than any other calculations (Gu 2005). Without knowing the proper line positions, spectral modeling is

beset by a host of potential problems. Flux may be assigned to the wrong transitions, ionization stages, or even elements. Lines calculated by any model are likely to be in the wrong place if they are not verified experimentally. An error of just 1% or 2% in the line positions has a tremendous effect on the predicted flux assignments, which is compounded if it leads to errors in line assignment. Such errors are likely given the great density of lines observed by *Chandra* and *XMM-Newton*.

Laboratory measurements are needed to locate the lines and to correlate them to the proper charge state. We have presented earlier extensive measurements of the L-shell emission spectra of argon (Lepson et al. 2003), following line lists of the iron L-shell emission in the soft X-ray band (Brown et al. 2002) and of the iron M-shell emission in the EUV (Lepson et al. 2002). We present here the L-shell emission spectra (transitions of the type $n'l' \rightarrow 2l$) of the sulfur ions S VII–S XIV in the wavelength range of 20–75 Å. Measurements concentrate on the strongest features in each charge state as these are the ones most likely to be observed in astrophysical plasmas. Our measurements are complemented by a full set of calculations from the Hebrew University–Lawrence Livermore Atomic Code (HULLAC; Bar-Shalom et al. 2001).

2. SPECTROSCOPIC MEASUREMENTS

Spectroscopic measurements were taken on the Lawrence Livermore electron beam ion traps EBIT-I and EBIT-II. EBIT-I and EBIT-II are well suited for such investigations because they can be operated at the low voltages (100–1000 eV) necessary to produce the charge states we investigated. Moreover, different charge states can be produced simply by changing the voltage of the electron beam. As the voltage increases, higher charge states appear when their ionization potentials are exceeded, and lower charge states decline and disappear as they become ionized. Ideally, charge states appear and disappear one by one as the voltage increases. In practice, there is some mixing because of recombination. Sulfur was introduced into the trap by a gas injection system. During this experiment we used a relatively high gas pressure to emphasize the lines. This continuous source of neutral sulfur resulted in the retention of the lower charge states even at higher beam energies. Consequently, spectra taken at the highest voltages contained all the charge states from S VII through S XIV. By systematically recording spectra at different energies and observing the rise and relative decline of different charge states, however, it is possible to determine which emission lines belong to which charge state.

Spectra were measured on EBIT-II with a grazing-incidence spectrometer (Utter et al. 1999) employing an average 2400 line mm^{-1} flat-field grating developed by Harada & Kita (1980) and Nakano et al. (1984) with a 1.3° angle of incidence, and an instrumental resolution of ~ 300 (at 25 Å) to ~ 500 (at 50 Å). Readouts were taken with a back-illuminated, liquid nitrogen-cooled CCD camera with a 1 inch square array of 1024×1024 pixels.

Wavelength calibrations were performed periodically throughout the experimental run using the well-known hydrogenic and helium-like K-shell emission lines of carbon, oxygen, and nitrogen. These lines were observed in first order and provided an accurate calibration region between 19 and 40 Å.

For calibration of wavelengths > 40 Å, we used the S VII lines $2p_{3/2}^5 3s_{1/2}^3 P_1$ (commonly labeled 3G) and $2p_{1/2}^5 3s^1 P_1$ (commonly labeled 3F), which we calibrated separately, using measurements taken on EBIT-I with a grazing-incidence spectrometer (Beiersdorfer et al. 1999a) employing an average 1200 line mm^{-1} flat-field grating developed by Harada & Kita (1980) and Nakano et al. (1984) with a 3° angle of incidence. Readouts were taken with a back-illuminated, liquid nitrogen-cooled CCD camera

with a 1 inch square array of 1024×1024 pixels. The instrumental resolution is ~ 300 at 100 Å. These spectra were calibrated using the well-known K-shell emission lines of nitrogen, in particular the N VII Ly α line and the N VI resonance line commonly referred to as w , as described by Beiersdorfer et al. (1999a). These lines were observed in the second through sixth orders (49–172 Å), and the S VII lines were measured in first and second orders.

Spectra were periodically taken without an active trap, i.e., without a potential applied to the trap electrodes. These spectra enabled us to determine the level of background emission (including visible light from the electron-gun filament, to which the CCD camera is sensitive), which was then subtracted from the sulfur spectra to yield background-corrected spectra.

After identification, we measured the relative fluxes of the emission lines for each charge state and corrected for differing sensitivity of the spectrometer (grating detector) at different wavelengths (Lepson et al. 2001). In the tables, the EBIT-II intensities given are corrected for the spectrometer sensitivity, but the HULLAC intensities are presented as calculated so that both are directly comparable to astronomical observations. We scaled the intensities to a maximum of 20, both to match our previously published work and because we feel this scale more accurately reflects the uncertainty of the intensity measurements.

3. THE SPECTRA

Figure 1 shows representative spectra of sulfur taken on EBIT-II at beam energies of 300, 450, and 750 eV, with the strongest sulfur lines labeled by charge state. Charge states from S VII through S XIV are present. The charge states can be identified by comparing spectra taken at different beam energies: as the beam energy increases, emission lines of higher charge states appear as their ionization thresholds are surpassed. Therefore, each new spectrum contains an additional, higher charge state. We measured at 10 energies between 200 and 750 eV, and additionally at 2 keV. Tables 1–8 present the major features for each charge state, along with our measured wavelengths and relative line strengths (intensity-corrected for spectrometer response). The tables also list predicted wavelengths and strengths from our present HULLAC code calculations, as well as the responsible line transition. We include lines from the two most widely used astronomical databases, MEKAL and CHIANTI, where those lines can be compared with the measured lines.

Line wavelengths in the HULLAC code are calculated in intermediate coupling and by means of the relativistic parametric potential method (Klapisch et al. 1977). Line intensities in the present work were calculated in the coronal steady state approximation assuming that the only important atomic processes within a given ionic state are electron impact excitation and spontaneous radiative decays. Radiative recombination was not included, as it is not important for the strong resonant lines under steady state conditions, even in a thermal plasma, and is likely negligible in the much narrower electron energy distribution found in electron beam ion traps. The electron energy distribution available for excitation is assumed to be Maxwellian, corresponding to an electron temperature ranging from $T_e = 600$ eV (for S VII–S IX) to $T_e = 1500$ eV (for S XII–S XIV). Calculations assumed a density of $5 \times 10^{11} \text{ cm}^{-3}$. We calculated nl with n up to 8 (for S X and S XI) or with n up to 10 (for all other charge states) and l up to “ d .” The total number of levels included was 289 for S VII, 883 for S VIII, 1738 for S IX, 1557 for S X, 1316 for S XI, 895 for S XII, 298 for S XIII, and 43 for S XIV. We used a Maxwellian model for its greater ease of calculation and because the model is sufficient for our goal of identifying the strong sulfur lines. The density and temperature values were chosen to best reflect the conditions found in EBIT-II.

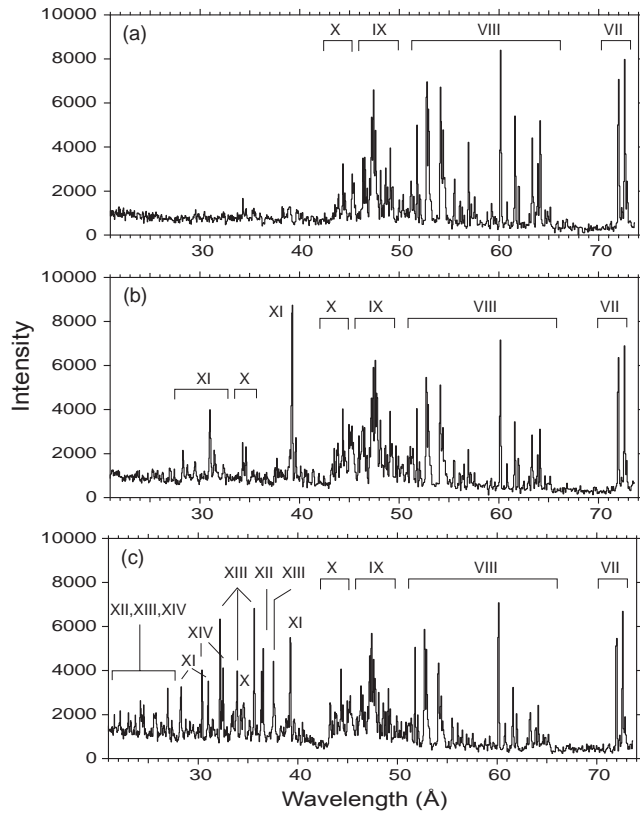


FIG. 1.—Spectra obtained with EBIT-II after subtraction of a constant stray light background. Note that each spectrum includes lines from several charge states. (a) Beam energy 300 eV. Dominant charge states are S VII, S VIII, and S IX. (b) Beam energy 450 eV. Charge states include S X and S XI. (c) Beam energy 730 eV. Charge states include S XII, S XIII, and S XIV.

Given the low densities at which the measurements were taken, line self-absorption in the trap is neglected.

4. COMPARISON WITH THEORY

We also constructed synthetic spectra derived from the HULLAC calculations that we overlaid onto the EBIT-II spectra. We did not adjust the EBIT-II spectra for the detector responsivity

in these figures, as this enhances unsightly noise in the regions where responsivity is low. Instead, we adjusted, for the figures only, the synthetic HULLAC spectra by the detector response so that they are directly comparable with our measurements.

Figures 2–9 show details of spectra from EBIT-II and compare them with the HULLAC calculations, covering all the charge states from S VII through S XIV. We make two representations of synthetic HULLAC spectra. In both cases, the spectra are intensity-corrected by the detector response function (see Fig. 1 in Lepson et al. 2003) and are normalized to the strongest EBIT-II peak in each charge state in order to make them directly comparable with the measured spectra. In the first overlay, no adjustments are made for differences in line position; this demonstrates the accuracy of the calculations for line identification. In the second overlay, we correct the position of each HULLAC line so that it coincides with the line as observed with EBIT-II; this is our best effort at adjusting theory to fit the laboratory measurements.

The HULLAC calculations do a reasonable job of reproducing the spectra observed on EBIT-II. In particular, most strong lines are rendered accurately enough to allow ready identification in our relatively simple spectra, which have just a single element, and in which we can distinguish between charge states taken at different beam energies. Yet even in this simplified system, it is often impossible to accurately assign the weaker emission lines: the wavelength accuracy of the calculations (Tables 1–8) is not sufficient to distinguish between the many weak lines, which are much harder to separate by charge state and are often clustered closer together than either the accuracy of the calculations or the resolution of the spectrometer. This situation does not change appreciably when performing a calculation for a monoenergetic electron beam, which would more closely match our conditions.

In Table 9 we make a cursory comparison of our laboratory measurements with the two most widely used databases, MEKAL and CHIANTI, noting the number of lines reported for each charge state investigated here. Both databases do best with the simplest, fewest electron systems of S XIV, and worse for the more complicated lower charge states, although MEKAL has some lines for all charge states and contains most of the lines we found in neon-like S VII.

TABLE 1
SUMMARY OF S VII EMISSION DATA

HULLAC Transition	HULLAC Intensity ^a	HULLAC λ (Å)	Feature	Measured Intensity ^a	Measured λ (Å)	Standard Error	MEKAL λ^c (Å)	MEKAL $\Delta\lambda^d$ (Å)
$(1s^2 2s_{1/2}^2 2p_{1/2} 2p_{3/2}^4 5d_{3/2})_1 \rightarrow (1s^2 2s_{1/2}^2 2p_{1/2}^2 2p_{3/2}^4)_0 \dots$	2	48.864	VII-1	3	48.639	0.003	0.225	...
	1	49.099	VII-2	2	48.866	0.004	0.233	...
$(1s^2 2s_{1/2}^2 2p_{1/2}^2 2p_{3/2}^4 3p_{1/2})_1 \rightarrow (1s^2 2s_{1/2}^2 2p_{1/2}^2 2p_{3/2}^4)_0 \dots$	1	49.628	VII-3	1	49.766	0.008	-0.138	50.000
$(1s^2 2s_{1/2}^2 2p_{1/2} 2p_{3/2}^4 4d_{3/2})_1 \rightarrow (1s^2 2s_{1/2}^2 2p_{1/2}^2 2p_{3/2}^4)_0 \dots$	6	52.020	VII-4	8	51.820	0.002	0.200	51.807
$(1s^2 2s_{1/2}^2 2p_{1/2}^2 2p_{3/2}^4 4d_{5/2})_1 \rightarrow (1s^2 2s_{1/2}^2 2p_{1/2}^2 2p_{3/2}^4)_0 \dots$	1	52.342	VII-5	3	52.112	0.008	0.230	52.097
$(1s^2 2s_{1/2}^2 2p_{1/2} 2p_{3/2}^4 3d_{3/2})_1 \rightarrow (1s^2 2s_{1/2}^2 2p_{1/2}^2 2p_{3/2}^4)_0 \dots$	20	60.338	VII-6	19	60.203	0.003	0.135	60.610
$(1s^2 2s_{1/2}^2 2p_{1/2}^2 2p_{3/2}^4 3d_{5/2})_1 \rightarrow (1s^2 2s_{1/2}^2 2p_{1/2}^2 2p_{3/2}^4)_0 \dots$	1	61.079	VII-7	3	60.851	0.003	0.228	60.807
	61.550	...
$(1s^2 2s_{1/2}^2 2p_{1/2} 2p_{3/2}^4 3s_{1/2})_1 \rightarrow (1s^2 2s_{1/2}^2 2p_{1/2}^2 2p_{3/2}^4)_0 \dots$	13	72.376	VII-8	20	72.032	0.002	0.344	72.027
$(1s^2 2s_{1/2}^2 2p_{1/2}^2 2p_{3/2}^4 3s_{1/2})_0 \rightarrow (1s^2 2s_{1/2}^2 2p_{1/2}^2 2p_{3/2}^4)_0 \dots$	VII-9	3	72.375	0.006
$(1s^2 2s_{1/2}^2 2p_{1/2}^2 2p_{3/2}^4 3s_{1/2})_1 \rightarrow (1s^2 2s_{1/2}^2 2p_{1/2}^2 2p_{3/2}^4)_0 \dots$	6	73.069	VII-10	18	72.662	0.002	0.407	72.663
$(1s^2 2s_{1/2}^2 2p_{1/2}^2 2p_{3/2}^4 3s_{1/2})_2 \rightarrow (1s^2 2s_{1/2}^2 2p_{1/2}^2 2p_{3/2}^4)_0 \dots$	5	73.317	VII-11	6	72.891	0.002	0.426	...

^a Relative to strongest peak; scale 1–20.

^b $\lambda_{\text{HULLAC}} - \lambda_{\text{EBIT}}$.

^c Kaastra & Mewe (1993); Mewe et al. (1995a).

^d $\lambda_{\text{MEKAL}} - \lambda_{\text{EBIT}}$.

TABLE 2
SUMMARY OF S VIII EMISSION DATA

HULLAC Transition	HULLAC Intensity ^a	HULLAC		Measured			MEKAL			Comment
		λ (Å)	Feature	Measured Intensity ^a	λ (Å)	Standard Error	$\Delta\lambda^b$ (Å)	$\Delta\lambda^d$ (Å)		
1048	$(1s^2 2s_{1/2}^2 2p_{1/2} 2p_{3/2}^2 5d_{3/2})_{3/2} \rightarrow (1s^2 2s_{1/2}^2 2p_{1/2}^2 2p_{3/2}^3)_{3/2}$	1	42.392	Carbon edge
	$(1s^2 2s_{1/2}^2 2p_{1/2} 2p_{3/2}^2 5d_{3/2})_{5/2} \rightarrow (1s^2 2s_{1/2}^2 2p_{1/2}^2 2p_{3/2}^3)_{3/2}$	1	42.398	Carbon edge
	$(1s^2 2s_{1/2}^2 2p_{3/2}^4 5d_{5/2})_{5/2} \rightarrow (1s^2 2s_{1/2}^2 2p_{1/2}^2 2p_{3/2}^3)_{3/2}$	2	42.332	Carbon edge
	$(1s^2 2s_{1/2}^2 2p_{1/2} 2p_{3/2}^2 4d_{5/2})_{5/2} \rightarrow (1s^2 2s_{1/2}^2 2p_{1/2}^2 2p_{3/2}^3)_{3/2}$	3	44.515	viii-1	5 ^e	44.386	0.002	0.129	...	Blend of three predicted lines
	$(1s^2 2s_{1/2}^2 2p_{1/2} 2p_{3/2}^2 4d_{5/2})_{3/2} \rightarrow (1s^2 2s_{1/2}^2 2p_{1/2}^2 2p_{3/2}^3)_{3/2}$	2	44.541	viii-1	5 ^e	44.386	0.002	0.155	...	Blend of three predicted lines
	$(1s^2 2s_{1/2}^2 2p_{1/2} 2p_{3/2}^2 4d_{3/2})_{1/2} \rightarrow (1s^2 2s_{1/2}^2 2p_{1/2}^2 2p_{3/2}^3)_{3/2}$	1	44.560	viii-1	5 ^e	44.386	0.002	0.174	...	Blend of three predicted lines
	$(1s^2 2s_{1/2}^2 2p_{1/2} 2p_{3/2}^2 4d_{3/2})_{3/2} \rightarrow (1s^2 2s_{1/2}^2 2p_{1/2}^2 2p_{3/2}^4)_{1/2}$	<1	44.685	viii-2	3 ^e	44.566	0.005	0.119	...	Blend of two predicted lines
	$(1s^2 2s_{1/2}^2 2p_{1/2} 2p_{3/2}^2 4d_{5/2})_{3/2} \rightarrow (1s^2 2s_{1/2}^2 2p_{1/2}^2 2p_{3/2}^4)_{1/2}$	1	44.734	viii-2	3 ^e	44.566	0.005	0.168	...	Blend of two predicted lines
	$(1s^2 2s_{1/2}^2 2p_{1/2} 2p_{3/2}^4 4d_{5/2})_{3/2} \rightarrow (1s^2 2s_{1/2}^2 2p_{1/2}^2 2p_{3/2}^3)_{3/2}$	6	45.468	viii-3	3	45.287	0.004	0.181	45.300	0.013
	$(1s^2 2s_{1/2}^2 2p_{1/2} 2p_{3/2}^2 4d_{3/2})_{3/2} \rightarrow (1s^2 2s_{1/2}^2 2p_{1/2}^2 2p_{3/2}^3)_{3/2}$	2	45.557	viii-4	7	45.457	0.005	0.100	46.000	0.543
	$(1s^2 2s_{1/2}^2 2p_{1/2} 2p_{3/2}^2 4s_{1/2})_{5/2} \rightarrow (1s^2 2s_{1/2}^2 2p_{1/2}^2 2p_{3/2}^3)_{3/2}$	2	46.565	viii-5	4	46.726	0.003	-0.161	...	Blend with ix
	$(1s^2 2s_{1/2}^2 2p_{1/2} 2p_{3/2}^2 3s_{1/2})_{5/2} \rightarrow (1s^2 2s_{1/2}^2 2p_{1/2}^2 2p_{3/2}^3)_{3/2}$	2	46.752	viii-6	4	46.789	0.002	-0.037
	viii-7	2	50.005	0.008
	$(1s^2 2s_{1/2}^2 2p_{1/2}^2 2p_{3/2}^2 3d_{5/2})_{5/2} \rightarrow (1s^2 2s_{1/2}^2 2p_{1/2}^2 2p_{3/2}^3)_{3/2}$	4	51.533	viii-8	3	51.272	0.008	0.261
	$(1s^2 2s_{1/2}^2 2p_{1/2}^2 2p_{3/2}^2 3d_{3/2})_{3/2} \rightarrow (1s^2 2s_{1/2}^2 2p_{1/2}^2 2p_{3/2}^4)_{1/2}$	<1	51.762	viii-9	2	51.469	0.007	0.293
	$(1s^2 2s_{1/2}^2 2p_{1/2} 2p_{3/2}^2 3d_{3/2})_{5/2} \rightarrow (1s^2 2s_{1/2}^2 2p_{1/2}^2 2p_{3/2}^3)_{3/2}$	20	52.884	viii-10	20	52.781	0.002	0.103	52.854	0.073
	$(1s^2 2s_{1/2}^2 2p_{1/2} 2p_{3/2}^2 3d_{5/2})_{3/2} \rightarrow (1s^2 2s_{1/2}^2 2p_{1/2}^2 2p_{3/2}^3)_{3/2}$	14	52.947	viii-11	14	52.973	0.002	-0.026
	$(1s^2 2s_{1/2}^2 2p_{1/2} 2p_{3/2}^3 3d_{5/2})_{3/2} \rightarrow (1s^2 2s_{1/2}^2 2p_{1/2}^2 2p_{3/2}^4)_{1/2}$	2	53.066	viii-12	2 ^e	53.222	0.009	-0.156	...	Blend of four predicted lines; shoulder of viii-11
	$(1s^2 2s_{1/2}^2 2p_{1/2} 2p_{3/2}^3 3d_{5/2})_{1/2} \rightarrow (1s^2 2s_{1/2}^2 2p_{1/2}^2 2p_{3/2}^4)_{1/2}$	2	53.125	viii-12	2 ^e	53.222	0.009	-0.097	...	Blend of four predicted lines; shoulder of viii-11
	$(1s^2 2s_{1/2}^2 2p_{1/2} 2p_{3/2}^2 3d_{5/2})_{3/2} \rightarrow (1s^2 2s_{1/2}^2 2p_{1/2}^2 2p_{3/2}^4)_{1/2}$	2	53.219	viii-12	2 ^e	53.222	0.009	-0.003	...	Blend of four predicted lines; shoulder of viii-11
	$(1s^2 2s_{1/2}^2 2p_{1/2} 2p_{3/2}^2 3d_{3/2})_{3/2} \rightarrow (1s^2 2s_{1/2}^2 2p_{1/2}^2 2p_{3/2}^3)_{3/2}$	5	53.233	viii-12	2 ^e	53.222	0.009	0.011	...	Blend of four predicted lines; shoulder of viii-11
	$(1s^2 2s_{1/2}^2 2p_{1/2}^4 2p_{3/2}^3 3d_{5/2})_{5/2} \rightarrow (1s^2 2s_{1/2}^2 2p_{1/2}^2 2p_{3/2}^3)_{3/2}$	16	54.312	viii-13	11	54.162	0.003	0.150	54.118	-0.044
	$(1s^2 2s_{1/2}^2 2p_{1/2}^2 2p_{3/2}^2 3d_{5/2})_{3/2} \rightarrow (1s^2 2s_{1/2}^2 2p_{1/2}^2 2p_{3/2}^3)_{3/2}$	3	54.471	viii-14	8 ^e	54.415	0.003	0.056	...	Blend of two predicted lines
	$(1s^2 2s_{1/2}^2 2p_{1/2} 2p_{3/2}^2 3d_{5/2})_{5/2} \rightarrow (1s^2 2s_{1/2}^2 2p_{1/2}^2 2p_{3/2}^3)_{3/2}$	3	54.589	viii-14	8 ^e	54.415	0.003	0.174	...	Blend of two predicted lines
	$(1s^2 2s_{1/2}^2 2p_{1/2}^2 2p_{3/2}^2 3d_{3/2})_{3/2} \rightarrow (1s^2 2s_{1/2}^2 2p_{1/2}^2 2p_{3/2}^4)_{1/2}$	2	54.759	viii-15	6	54.601	0.003	0.158
	$(1s^2 2s_{1/2}^2 2p_{1/2}^2 2p_{3/2}^2 3s_{1/2})_{1/2} \rightarrow (1s^2 2s_{1/2}^2 2p_{1/2}^2 2p_{3/2}^3)_{3/2}$	2	59.698	viii-16	3	59.308	0.004	0.390
	$(1s^2 2s_{1/2}^2 2p_{1/2}^2 2p_{3/2}^2 3s_{1/2})_{1/2} \rightarrow (1s^2 2s_{1/2}^2 2p_{1/2}^2 2p_{3/2}^4)_{1/2}$	2	60.044	viii-17	2	59.624	0.013	0.420
	$(1s^2 2s_{1/2}^2 2p_{1/2} 2p_{3/2}^2 3s_{1/2})_{5/2} \rightarrow (1s^2 2s_{1/2}^2 2p_{1/2}^2 2p_{3/2}^3)_{3/2}$	17	61.866	viii-18	15	61.645	0.002	0.221	61.600	-0.045
	$(1s^2 2s_{1/2}^2 2p_{1/2} 2p_{3/2}^2 3s_{1/2})_{3/2} \rightarrow (1s^2 2s_{1/2}^2 2p_{1/2}^2 2p_{3/2}^4)_{1/2}$	4	62.232	viii-19	6	62.029	0.001	0.203
	$(1s^2 2s_{1/2}^2 2p_{1/2} 2p_{3/2}^2 3s_{1/2})_{3/2} \rightarrow (1s^2 2s_{1/2}^2 2p_{1/2}^2 2p_{3/2}^3)_{3/2}$	2	63.332	viii-20	2	63.061	0.004	0.271
	$(1s^2 2s_{1/2}^2 2p_{1/2} 2p_{3/2}^2 3s_{1/2})_{3/2} \rightarrow (1s^2 2s_{1/2}^2 2p_{1/2}^2 2p_{3/2}^3)_{3/2}$	16	63.608	viii-21	10 ^e	63.365	0.002	0.243	63.204	-0.061
	$(1s^2 2s_{1/2}^2 2p_{1/2} 2p_{3/2}^2 3s_{1/2})_{1/2} \rightarrow (1s^2 2s_{1/2}^2 2p_{1/2}^2 2p_{3/2}^4)_{1/2}$	3	63.722	viii-21	10 ^e	63.365	0.002	0.357	63.304	-0.061
	$(1s^2 2s_{1/2}^2 2p_{1/2}^2 2p_{3/2}^2 3s_{1/2})_{3/2} \rightarrow (1s^2 2s_{1/2}^2 2p_{1/2}^2 2p_{3/2}^4)_{1/2}$	2	64.001	viii-22	2	63.784	0.010	0.217
	$(1s^2 2s_{1/2}^2 2p_{1/2} 2p_{3/2}^2 3s_{1/2})_{3/2} \rightarrow (1s^2 2s_{1/2}^2 2p_{1/2}^2 2p_{3/2}^3)_{3/2}$	5	64.299	viii-23	7	63.935	0.003	0.364
	$(1s^2 2s_{1/2}^2 2p_{1/2}^2 2p_{3/2}^2 3s_{1/2})_{5/2} \rightarrow (1s^2 2s_{1/2}^2 2p_{1/2}^2 2p_{3/2}^3)_{3/2}$	8	64.536	viii-24	16 ^e	64.185	0.002	0.351	...	Blend of two predicted lines
	$(1s^2 2s_{1/2}^2 2p_{1/2}^4 2p_{3/2}^3 3s_{1/2})_{1/2} \rightarrow (1s^2 2s_{1/2}^2 2p_{1/2}^2 2p_{3/2}^4)_{1/2}$	2	64.553	viii-24	16 ^e	64.185	0.002	0.368	...	Blend of two predicted lines
	$(1s^2 2s_{1/2}^2 2p_{1/2}^2 2p_{3/2}^3 3s_{1/2})_{3/2} \rightarrow (1s^2 2s_{1/2}^2 2p_{1/2}^2 2p_{3/2}^4)_{1/2}$	4	65.725	viii-25	3	65.194	0.005	0.531

^a Relative to strongest peak; scale 1–20.

^b $\lambda_{\text{HULLAC}} - \lambda_{\text{EBIT}}$.

^c Kaastra & Mewe (1993); Mewe et al. (1995a).

^d $\lambda_{\text{MEKAL}} - \lambda_{\text{EBIT}}$.

^e Combined intensity of blended feature.

TABLE 3
SUMMARY OF S IX EMISSION DATA

HULLAC Transition	HULLAC Intensity ^a	HULLAC		Measured			MEKAL			Comment
		λ (Å)	Feature	Measured Intensity ^a	λ (Å)	Standard Error	λ^c (Å)	$\Delta\lambda^d$		
$(1s^2 2s_{1/2}^2 2p_{3/2}^2 5d_{5/2})_6 \rightarrow (1s^2 2s_{1/2}^2 2p_{1/2}^2 2p_{3/2}^2)_4$	1	35.559
$(1s^2 2s_{1/2}^2 2p_{3/2}^2 6d_{3/2})_6 \rightarrow (1s^2 2s_{1/2}^2 2p_{1/2}^2 2p_{3/2}^2)_4$	1	35.722
$(1s^2 2s_{1/2}^2 2p_{1/2} 2p_{3/2}^2 5d_{3/2})_4 \rightarrow (1s^2 2s_{1/2}^2 2p_{1/2}^2 2p_{3/2}^2)_4$	1	36.071
$(1s^2 2s_{1/2}^2 2p_{1/2} 2p_{3/2}^2 5d_{5/2})_6 \rightarrow (1s^2 2s_{1/2}^2 2p_{1/2}^2 2p_{3/2}^2)_4$	1	36.106
$(1s^2 2s_{1/2}^2 2p_{1/2} 2p_{3/2}^2 5d_{5/2})_6 \rightarrow (1s^2 2s_{1/2}^2 2p_{1/2}^2 2p_{3/2}^2)_4$	2	37.192
$(1s^2 2s_{1/2}^2 2p_{1/2} 2p_{3/2}^2 4d_{5/2})_6 \rightarrow (1s^2 2s_{1/2}^2 2p_{1/2}^2 2p_{3/2}^2)_4$	2	38.419
$(1s^2 2s_{1/2}^2 2p_{3/2}^2 4d_{3/2})_2 \rightarrow (1s^2 2s_{1/2}^2 2p_{1/2}^2 2p_{3/2}^2)_4$	1	38.929	IX-1	1 ^e	39.085	0.007	-0.156	39.460	0.375	Blend of three predicted lines
$(1s^2 2s_{1/2}^2 2p_{1/2} 2p_{3/2}^2 4d_{5/2})_4 \rightarrow (1s^2 2s_{1/2}^2 2p_{1/2}^2 2p_{3/2}^2)_4$	3	38.996	IX-1	1 ^e	39.085	0.007	-0.089	39.460	0.375	Blend of three predicted lines
$(1s^2 2s_{1/2}^2 2p_{1/2} 2p_{3/2}^2 4d_{5/2})_6 \rightarrow (1s^2 2s_{1/2}^2 2p_{1/2}^2 2p_{3/2}^2)_4$	3	39.06	IX-1	1 ^e	39.085	0.007	-0.025	39.460	0.375	Blend of three predicted lines
$(1s^2 2s_{1/2}^2 2p_{1/2}^2 2p_{3/2}^2 3p_{3/2})_6 \rightarrow (1s^2 2s_{1/2}^2 2p_{1/2}^2 2p_{3/2}^2)_4$	1	39.508
$(1s^2 2s_{1/2}^2 2p_{1/2} 2p_{3/2}^2 4p_{3/2})_6 \rightarrow (1s^2 2s_{1/2}^2 2p_{1/2}^2 2p_{3/2}^2)_4$	4	40.277
$(1s^2 2s_{1/2}^2 2p_{1/2}^2 2p_{3/2}^2 4d_{5/2})_4 \rightarrow (1s^2 2s_{1/2}^2 2p_{1/2}^2 2p_{3/2}^2)_2$	1	40.404
$(1s^2 2s_{1/2}^2 2p_{1/2} 2p_{3/2}^2 4s_{1/2})_6 \rightarrow (1s^2 2s_{1/2}^2 2p_{1/2}^2 2p_{3/2}^2)_4$	1	40.584
$(1s^2 2s_{1/2}^2 2p_{1/2} 2p_{3/2}^2 3p_{1/2})_4 \rightarrow (1s^2 2s_{1/2}^2 2p_{1/2}^2 2p_{3/2}^2)_4$	1	43.706
$(1s^2 2s_{1/2}^2 2p_{1/2} 2p_{3/2}^2 3p_{1/2})_4 \rightarrow (1s^2 2s_{1/2}^2 2p_{1/2}^2 2p_{3/2}^2)_2$	1	43.847	IX-2	1 ^e	43.765	0.011	0.082	Blend of two predicted lines, with x
$(1s^2 2s_{1/2}^2 2p_{1/2}^2 2p_{3/2}^2 3p_{1/2})_2 \rightarrow (1s^2 2s_{1/2}^2 2p_{1/2}^2 2p_{3/2}^2)_4$	1	43.877	IX-2	1 ^e	43.765	0.011	0.112	Blend of two predicted lines, with x
$(1s^2 2s_{1/2}^2 2p_{1/2}^2 2p_{3/2}^2 3p_{1/2})_6 \rightarrow (1s^2 2s_{1/2}^2 2p_{1/2}^2 2p_{3/2}^2)_4$	4	44.066	IX-3	1	43.891	0.007	0.175	Blend with x
$(1s^2 2s_{1/2}^2 2p_{1/2} 2p_{3/2}^2 3p_{1/2})_6 \rightarrow (1s^2 2s_{1/2}^2 2p_{1/2}^2 2p_{3/2}^2)_4$	1	44.115
$(1s^2 2s_{1/2}^2 2p_{1/2} 2p_{3/2}^2 3p_{1/2})_4 \rightarrow (1s^2 2s_{1/2}^2 2p_{1/2}^2 2p_{3/2}^2)_2$	1	45.453
$(1s^2 2s_{1/2}^2 2p_{1/2} 2p_{3/2}^2 3d_{5/2})_6 \rightarrow (1s^2 2s_{1/2}^2 2p_{1/2}^2 2p_{3/2}^2)_4$	10	46.535	IX-4	7	46.383	0.004	0.152
$(1s^2 2s_{1/2}^2 2p_{1/2} 2p_{3/2}^2 3d_{5/2})_4 \rightarrow (1s^2 2s_{1/2}^2 2p_{1/2}^2 2p_{3/2}^2)_2$	2	46.726	...	3	46.592	0.003	0.134	Blend with viii-6
$(1s^2 2s_{1/2}^2 2p_{1/2} 2p_{3/2}^2 3d_{5/2})_6 \rightarrow (1s^2 2s_{1/2}^2 2p_{1/2}^2 2p_{3/2}^2)_4$	1	46.801
$(1s^2 2s_{1/2}^2 2p_{1/2}^2 2p_{3/2}^2 3d_{5/2})_2 \rightarrow (1s^2 2s_{1/2}^2 2p_{1/2}^2 2p_{3/2}^2)_4$	4	47.178
$(1s^2 2s_{1/2}^2 2p_{1/2} 2p_{3/2}^2 3d_{3/2})_2 \rightarrow (1s^2 2s_{1/2}^2 2p_{1/2}^2 2p_{3/2}^2)_4$	3	47.333	IX-5	3	47.078	0.005	0.255
$(1s^2 2s_{1/2}^2 2p_{1/2}^2 2p_{3/2}^2 3d_{3/2})_2 \rightarrow (1s^2 2s_{1/2}^2 2p_{1/2} 2p_{3/2}^2)_2$	2	47.342
$(1s^2 2s_{1/2}^2 2p_{1/2}^2 2p_{3/2}^2 3d_{5/2})_2 \rightarrow (1s^2 2s_{1/2}^2 2p_{1/2} 2p_{3/2}^2)_0$	1	47.406
$(1s^2 2s_{1/2}^2 2p_{1/2}^2 2p_{3/2}^2 3d_{5/2})_4 \rightarrow (1s^2 2s_{1/2}^2 2p_{1/2}^2 2p_{3/2}^2)_2$	16	47.41	IX-6	16	47.256	0.004	0.154
$(1s^2 2s_{1/2}^2 2p_{1/2} 2p_{3/2}^2 3d_{3/2})_2 \rightarrow (1s^2 2s_{1/2}^2 2p_{1/2}^2 2p_{3/2}^2)_2$	1	47.498
$(1s^2 2s_{1/2}^2 2p_{1/2} 2p_{3/2}^2 3d_{3/2})_6 \rightarrow (1s^2 2s_{1/2}^2 2p_{1/2}^2 2p_{3/2}^2)_4$	20	47.521	IX-7	20	47.436	0.001	0.085	47.500	0.064	...
$(1s^2 2s_{1/2}^2 2p_{1/2} 2p_{3/2}^2 3d_{3/2})_2 \rightarrow (1s^2 2s_{1/2}^2 2p_{1/2}^2 2p_{3/2}^4)_0$	1	47.562
$(1s^2 2s_{1/2}^2 2p_{3/2}^2 3d_{3/2})_4 \rightarrow (1s^2 2s_{1/2}^2 2p_{1/2}^2 2p_{3/2}^2)_2$	2	47.576
$(1s^2 2s_{1/2}^2 2p_{1/2} 2p_{3/2}^2 3d_{5/2})_4 \rightarrow (1s^2 2s_{1/2}^2 2p_{1/2}^2 2p_{3/2}^2)_2$	1	47.711
$(1s^2 2s_{1/2}^2 2p_{1/2} 2p_{3/2}^2 3d_{5/2})_6 \rightarrow (1s^2 2s_{1/2}^2 2p_{1/2}^2 2p_{3/2}^2)_4$	1	48.193	IX-8	3	47.818	0.013	0.375
$(1s^2 2s_{1/2}^2 2p_{1/2}^2 2p_{3/2}^2 3d_{5/2})_6 \rightarrow (1s^2 2s_{1/2}^2 2p_{1/2}^2 2p_{3/2}^2)_4$	1	48.299	IX-9	7	48.158	0.002	0.141

TABLE 3—Continued

HULLAC Transition	HULLAC Intensity ^a	HULLAC		Measured		MEKAL			Comment
		λ (Å)	Feature	Measured Intensity ^a	λ (Å)	Standard Error	$\Delta\lambda^b$ (Å)	$\Delta\lambda^d$ (Å)	
(1s ² 2s _{1/2} ² 2p _{1/2} ² 2p _{3/2} ² 4p _{3/2}) ₄ → (1s ² 2s _{1/2} ² 2p _{1/2} ² 2p _{3/2} ³) ₄	1	48.465	ix-10	2	48.377	0.006	0.088
(1s ² 2s _{1/2} ² 2p _{1/2} ² 2p _{3/2} ² 3d _{5/2}) ₆ → (1s ² 2s _{1/2} ² 2p _{1/2} ² 2p _{3/2} ²) ₄	13	49.265	ix-11	9 ^e	49.127	0.003	0.138	...	Blend of two predicted lines
(1s ² 2s _{1/2} ² 2p _{1/2} ² 2p _{3/2} ² 3d _{5/2}) ₄ → (1s ² 2s _{1/2} ² 2p _{1/2} ² 2p _{3/2} ²) ₄	1	49.284	ix-11	9 ^e	49.127	0.003	0.157	...	Blend of two predicted lines
(1s ² 2s _{1/2} ² 2p _{1/2} ² 2p _{3/2} ² 3d _{5/2}) ₄ → (1s ² 2s _{1/2} ² 2p _{1/2} ² 2p _{3/2} ²) ₂	2	49.463	ix-12	6	49.326	0.004	0.137
(1s ² 2s _{1/2} ² 2p _{1/2} ² 2p _{3/2} ² 4p _{3/2}) ₄ → (1s ² 2s _{1/2} ² 2p _{1/2} ² 2p _{3/2} ⁴) ₂	1	50.46
(1s ² 2s _{1/2} ² 2p _{1/2} ² 2p _{3/2} ² 3d _{5/2}) ₆ → (1s ² 2s _{1/2} ² 2p _{1/2} ² 2p _{3/2} ²) ₄	1	50.641
(1s ² 2p _{1/2} ² 2p _{3/2} ⁴) ₂ → (1s ² 2s _{1/2} ² 2p _{1/2} ² 2p _{3/2} ²) ₄	2	50.766	ix-13	7	50.398	0.006	0.368
(1s ² 2s _{1/2} ² 2p _{1/2} ² 2p _{3/2} ³ d _{5/2}) ₄ → (1s ² 2s _{1/2} ² 2p _{1/2} ² 2p _{3/2} ²) ₂	1	50.781
(1s ² 2s _{1/2} ² 2p _{1/2} ² 2p _{3/2} ³ d _{5/2}) ₆ → (1s ² 2s _{1/2} ² 2p _{1/2} ² 2p _{3/2} ²) ₄	1	51.063
(1s ² 2s _{1/2} ² 2p _{1/2} ² 2p _{3/2} ³ s _{1/2}) ₄ → (1s ² 2s _{1/2} ² 2p _{1/2} ² 2p _{3/2} ²) ₄	2	53.162	52.973	0.002	0.189	...	Blend with viii-10
(1s ² 2s _{1/2} ² 2p _{1/2} ² 2p _{3/2} ³ s _{1/2}) ₆ → (1s ² 2s _{1/2} ² 2p _{1/2} ² 2p _{3/2} ²) ₄	2	53.37	Blend of two predicted lines, with viii-11
(1s ² 2s _{1/2} ² 2p _{1/2} ² 2p _{3/2} ² 3s _{1/2}) ₂ → (1s ² 2s _{1/2} ² 2p _{1/2} ² 2p _{3/2} ⁴) ₀	1	53.504	Blend of two predicted lines, with viii-11
(1s ² 2s _{1/2} ² 2p _{1/2} ² 2p _{3/2} ² 3s _{1/2}) ₆ → (1s ² 2s _{1/2} ² 2p _{1/2} ² 2p _{3/2} ²) ₄	12	54.37	54.162	0.003	0.208	54.180	0.018 Blend with viii-13
(1s ² 2s _{1/2} ² 2p _{1/2} ² 2p _{3/2} ² 3s _{1/2}) ₄ → (1s ² 2s _{1/2} ² 2p _{1/2} ² 2p _{3/2} ²) ₄	2	54.4
(1s ² 2s _{1/2} ² 2p _{1/2} ² 2p _{3/2} ² 3s _{1/2}) ₄ → (1s ² 2s _{1/2} ² 2p _{1/2} ² 2p _{3/2} ²) ₂	2	54.618	54.415	0.003	0.203	...	Blend with viii-14
(1s ² 2s _{1/2} ² 2p _{1/2} ² 2p _{3/2} ³ s _{1/2}) ₄ → (1s ² 2s _{1/2} ² 2p _{1/2} ² 2p _{3/2} ²) ₄	1	54.966
(1s ² 2s _{1/2} ² 2p _{1/2} ² 2p _{3/2} ² 3s _{1/2}) ₄ → (1s ² 2s _{1/2} ² 2p _{1/2} ² 2p _{3/2} ²) ₄	2	55.799	ix-14	5	55.561	0.002	0.238
(1s ² 2s _{1/2} ² 2p _{1/2} ² 2p _{3/2} ² 3s _{1/2}) ₂ → (1s ² 2s _{1/2} ² 2p _{1/2} ² 2p _{3/2} ²) ₄	5	56.316	ix-15	3	56.108	0.002	0.208
(1s ² 2s _{1/2} ² 2p _{1/2} ² 2p _{3/2} ² 3s _{1/2}) ₄ → (1s ² 2s _{1/2} ² 2p _{1/2} ² 2p _{3/2} ²) ₂	3	56.55	ix-16	2	56.369	0.012	0.181
(1s ² 2s _{1/2} ² 2p _{1/2} ² 2p _{3/2} ² 3s _{1/2}) ₂ → (1s ² 2s _{1/2} ² 2p _{1/2} ² 2p _{3/2} ⁴) ₀	1	56.641
(1s ² 2s _{1/2} ² 2p _{1/2} ² 2p _{3/2} ² 3s _{1/2}) ₄ → (1s ² 2s _{1/2} ² 2p _{1/2} ² 2p _{3/2} ²) ₄	5	57.322	ix-17	8	56.986	0.003	0.336
(1s ² 2s _{1/2} ² 2p _{1/2} ² 2p _{3/2} ² 3s _{1/2}) ₄ → (1s ² 2s _{1/2} ² 2p _{1/2} ² 2p _{3/2} ²) ₂	1	57.564	ix-18	3	57.218	0.001	0.346
(1s ² 2s _{1/2} ² 2p _{1/2} ² 2p _{3/2} ² 3s _{1/2}) ₄ → (1s ² 2s _{1/2} ² 2p _{1/2} ² 2p _{3/2} ²) ₄	5	57.991	ix-19	3 ^e	57.583	0.004	0.408	...	Blend of two predicted lines
(1s ² 2s _{1/2} ² 2p _{1/2} ² 2p _{3/2} ² 3s _{1/2}) ₄ → (1s ² 2s _{1/2} ² 2p _{1/2} ² 2p _{3/2} ²) ₂	2	58.219	ix-19	3 ^e	57.583	0.004	0.636	...	Blend of two predicted lines
...	...	ix-20	2	58.851	0.006
(1s ² 2s _{1/2} ² 2p _{1/2} ² 2p _{3/2} ² 3p _{3/2}) ₄ → (1s ² 2s _{1/2} ² 2p _{1/2} ² 2p _{3/2} ³) ₄	1	64.181
(1s ² 2s _{1/2} ² 2p _{1/2} ² 2p _{3/2} ² 3p _{3/2}) ₄ → (1s ² 2s _{1/2} ² 2p _{1/2} ² 2p _{3/2} ³) ₂	4	65.118	ix-21	2	64.697	0.004	0.421
(1s ² 2s _{1/2} ² 2p _{1/2} ² 2p _{3/2} ² 3p _{3/2}) ₄ → (1s ² 2s _{1/2} ² 2p _{1/2} ² 2p _{3/2} ⁴) ₂	1	65.405	ix-22	2	64.926	0.010	0.479

^a Relative to strongest peak; scale 1–20.^b $\lambda_{\text{HULLAC}} - \lambda_{\text{EBIT}}$.^c Kaastra & Mewe (1993); Mewe et al. (1995b).^d $\lambda_{\text{MEKAL}} - \lambda_{\text{EBIT}}$.^e Combined intensity of blended feature.

TABLE 4
SUMMARY OF S X EMISSION DATA

HULLAC Transition	HULLAC Intensity ^a	HULLAC λ (Å)	Feature	Measured Intensity ^a	λ (Å)	Standard Error	MEKAL λ^c (Å)	CHIANTI λ^e (Å)	Comment
							$\Delta\lambda^b$	$\Delta\lambda^d$	
(1s ² 2s _{1/2} ² 2p _{1/2} ² p _{3/2} ⁵ d _{5/2}) _{3/2} → (1s ² 2s _{1/2} ² p _{1/2} ² p _{3/2} ²) _{3/2}	1	31.596	x-1	6	31.511	0.007	0.085
(1s ² 2p _{3/2} ⁴ d _{5/2}) _{5/2} → (1s ² 2s _{1/2} ² p _{1/2} ² p _{3/2} ²) _{3/2}	1	31.606
(1s ² 2s _{1/2} ² p _{3/2} ² p _{3/2} ⁴ p _{1/2}) _{5/2} → (1s ² 2s _{1/2} ² p _{1/2} ² p _{3/2} ²) _{3/2}	1	32.933	x-2	1	32.407	0.007	0.526
(1s ² 2s _{1/2} ² p _{3/2} ² 4d _{5/2}) _{1/2} → (1s ² 2s _{1/2} ² p _{1/2} ² p _{3/2} ²) _{3/2}	1	34.377	x-3	6 ^f	34.319	0.003	0.058
(1s ² 2s _{1/2} ² p _{3/2} ² 4d _{5/2}) _{3/2} → (1s ² 2s _{1/2} ² p _{1/2} ² p _{3/2} ²) _{3/2}	2	34.388	x-3	6 ^f	34.319	0.003	0.069
(1s ² 2s _{1/2} ² p _{3/2} ² 4d _{5/2}) _{5/2} → (1s ² 2s _{1/2} ² p _{1/2} ² p _{3/2} ²) _{3/2}	1	34.408	x-3	6 ^f	34.319	0.003	0.089
(1s ² 2s _{1/2} ² p _{1/2} ² p _{3/2} ⁴ d _{3/2}) _{5/2} → (1s ² 2s _{1/2} ² p _{1/2} ² p _{3/2} ²) _{3/2}	1	34.506	x-4	3	34.44	0.011	0.066
(1s ² 2s _{1/2} ² p _{1/2} ² p _{3/2} ² 4d _{3/2}) _{5/2} → (1s ² 2s _{1/2} ² p _{1/2} ² p _{3/2} ²) _{3/2}	1	34.767	x-5	6 ^f	34.623	0.009	0.144
(1s ² 2s _{1/2} ² p _{1/2} ² p _{3/2} ² 4d _{3/2}) _{7/2} → (1s ² 2s _{1/2} ² p _{1/2} ² p _{3/2} ²) _{5/2}	1	34.792	x-5	6 ^f	34.623	0.009	0.169
(1s ² 2s _{1/2} ² p _{3/2} ² 4d _{5/2}) _{7/2} → (1s ² 2s _{1/2} ² p _{1/2} ² p _{3/2} ²) _{5/2}	1	35.411	x-6	1	35.278	0.006	0.133
(1s ² 2s _{1/2} ² p _{1/2} ² p _{3/2} ⁴ d _{5/2}) _{5/2} → (1s ² 2s _{1/2} ² p _{1/2} ² p _{3/2} ²) _{3/2}	1	35.494	x-7	1	35.455	0.007	0.039
(1s ² 2s _{1/2} ² p _{3/2} ² 4d _{5/2}) _{5/2} → (1s ² 2s _{1/2} ² p _{3/2} ²) _{3/2}	<1	35.849	x-8	1	35.756	0.006	0.093
	x-9	1	35.996	0.003
(1s ² 2s _{1/2} ² p _{1/2} ² p _{3/2} ³ p _{3/2}) _{5/2} → (1s ² 2s _{1/2} ² p _{1/2} ² p _{3/2} ²) _{3/2}	1	36.489	36.900
(1s ² 2s _{1/2} ² p _{1/2} ² p _{3/2} ³ p _{3/2}) _{3/2} → (1s ² 2s _{1/2} ² p _{1/2} ² p _{3/2} ²) _{3/2}	1	39.711	Blend of two predicted lines, with viii
(1s ² 2s _{1/2} ² p _{1/2} ² p _{3/2} ³ p _{3/2}) _{5/2} → (1s ² 2s _{1/2} ² p _{1/2} ² p _{3/2} ²) _{5/2}	1	39.741	Blend of two predicted lines, with viii
(1s ² 2s _{1/2} ² p _{1/2} ² p _{3/2} ³ p _{3/2}) _{7/2} → (1s ² 2s _{1/2} ² p _{1/2} ² p _{3/2} ²) _{3/2}	1	40.278	x-10	1 ^f	40.211	0.0098	0.067
(1s ² 2s _{1/2} ² p _{1/2} ² p _{3/2} ³ p _{3/2}) _{7/2} → (1s ² 2s _{1/2} ² p _{1/2} ² p _{3/2} ²) _{5/2}	1	40.311	x-10	1 ^f	40.211	0.0098	0.100
(1s ² 2s _{1/2} ² p _{1/2} ² p _{3/2} ³ p _{3/2}) _{1/2} → (1s ² 2s _{1/2} ² p _{1/2} ² p _{3/2} ²) _{3/2}	1	41.545	x-11	9 ^f	41.363	0.022	0.182
(1s ² 2s _{1/2} ² p _{1/2} ² p _{3/2} ³ p _{3/2}) _{3/2} → (1s ² 2s _{1/2} ² p _{1/2} ² p _{3/2} ²) _{3/2}	2	41.551	x-11	9 ^f	41.363	0.022	0.188
(1s ² 2s _{1/2} ² p _{1/2} ² p _{3/2} ³ p _{3/2}) _{5/2} → (1s ² 2s _{1/2} ² p _{1/2} ² p _{3/2} ²) _{3/2}	2	41.558	x-11	9	41.363	0.022	0.195
(1s ² 2s _{1/2} ² p _{3/2} ³ d _{5/2}) _{1/2} → (1s ² 2s _{1/2} ² p _{1/2} ² p _{3/2} ²) _{3/2}	7	42.581	42.5430	Carbon edge
(1s ² 2s _{1/2} ² p _{3/2} ³ d _{5/2}) _{3/2} → (1s ² 2s _{1/2} ² p _{1/2} ² p _{3/2} ²) _{3/2}	14	42.605	Carbon edge
(1s ² 2s _{1/2} ² p _{3/2} ³ d _{5/2}) _{5/2} → (1s ² 2s _{1/2} ² p _{1/2} ² p _{3/2} ²) _{3/2}	20	42.653	42.530	...	Carbon edge
(1s ² 2s _{1/2} ² p _{3/2} ³ d _{5/2}) _{7/2} → (1s ² 2s _{1/2} ² p _{1/2} ² p _{3/2} ²) _{1/2}	1	42.768	Carbon edge
(1s ² 2s _{1/2} ² p _{3/2} ³ d _{5/2}) _{5/2} → (1s ² 2s _{1/2} ² p _{3/2} ²) _{3/2}	2	42.846	Carbon edge
(1s ² 2s _{1/2} ² p _{3/2} ³ d _{5/2}) _{7/2} → (1s ² 2s _{1/2} ² p _{3/2} ²) _{3/2}	2	42.917	Carbon edge
(1s ² 2s _{1/2} ² p _{3/2} ³ d _{5/2}) _{5/2} → (1s ² 2s _{1/2} ² p _{3/2} ²) _{3/2}	5	43.019	Carbon edge
(1s ² 2s _{1/2} ² p _{1/2} ² p _{3/2} ³ d _{5/2}) _{7/2} → (1s ² 2s _{1/2} ² p _{1/2} ² p _{3/2} ²) _{5/2}	10	43.097	43.002	...	Carbon edge
(1s ² 2s _{1/2} ² p _{1/2} ² p _{3/2} ³ d _{5/2}) _{1/2} → (1s ² 2s _{1/2} ² p _{1/2} ² p _{3/2} ²) _{3/2}	1	43.147	Carbon edge
(1s ² 2s _{1/2} ² p _{1/2} ² p _{3/2} ³ d _{5/2}) _{3/2} → (1s ² 2s _{1/2} ² p _{1/2} ² p _{3/2} ²) _{3/2}	1	43.175	Carbon edge
(1s ² 2s _{1/2} ² p _{1/2} ² p _{3/2} ³ d _{5/2}) _{5/2} → (1s ² 2s _{1/2} ² p _{1/2} ² p _{3/2} ²) _{3/2}	2	43.176	Carbon edge
(1s ² 2s _{1/2} ² p _{1/2} ² p _{3/2} ³ d _{5/2}) _{7/2} → (1s ² 2s _{1/2} ² p _{1/2} ² p _{3/2} ²) _{5/2}	1	43.352	Carbon edge
(1s ² 2s _{1/2} ² p _{1/2} ² p _{3/2} ³ d _{5/2}) _{3/2} → (1s ² 2s _{1/2} ² p _{3/2} ²) _{3/2}	1	43.650	x-12	8 ^f	43.544	0.002	0.106
(1s ² 2s _{1/2} ² p _{1/2} ² p _{3/2} ³ d _{5/2}) _{5/2} → (1s ² 2s _{1/2} ² p _{3/2} ²) _{3/2}	1	43.658	x-12	8 ^f	43.544	0.002	0.114
(1s ² 2s _{1/2} ² p _{1/2} ² p _{3/2} ³ d _{5/2}) _{1/2} → (1s ² 2s _{1/2} ² p _{1/2} ² p _{3/2} ²) _{1/2}	1	43.66	x-12	8 ^f	43.544	0.002	0.116
(1s ² 2s _{1/2} ² p _{1/2} ² p _{3/2} ³ d _{5/2}) _{5/2} → (1s ² 2s _{1/2} ² p _{1/2} ² p _{3/2} ²) _{5/2}	2	43.688	x-12	8 ^f	43.544	0.002	0.144
(1s ² 2s _{1/2} ² p _{3/2} ³ d _{5/2}) _{3/2} → (1s ² 2s _{1/2} ² p _{1/2} ² p _{3/2} ²) _{3/2}	1	43.692	x-12	8 ^f	43.544	0.002	0.148
(1s ² 2s _{1/2} ² p _{3/2} ³ d _{5/2}) _{5/2} → (1s ² 2s _{1/2} ² p _{3/2} ²) _{3/2}	2	43.842	x-13	5	43.765	0.011	0.077
(1s ² 2s _{1/2} ² p _{3/2} ³ d _{5/2}) _{3/2} → (1s ² 2s _{1/2} ² p _{1/2} ² p _{3/2} ²) _{1/2}	1	43.964	x-14	6	43.859	0.011	0.105
(1s ² 2s _{1/2} ² p _{3/2} ³ d _{5/2}) _{5/2} → (1s ² 2s _{1/2} ² p _{1/2} ² p _{3/2} ²) _{3/2}	2	43.975	x-14	6	43.859	0.011	0.116
(1s ² 2s _{1/2} ² p _{3/2} ³ d _{5/2}) _{7/2} → (1s ² 2s _{1/2} ² p _{1/2} ² p _{3/2} ²) _{5/2}	2	44.259	x-15	2	44.093	0.002	0.166
(1s ² 2s _{1/2} ² p _{1/2} ² p _{3/2} ³ d _{5/2}) _{5/2} → (1s ² 2s _{1/2} ² p _{1/2} ² p _{3/2} ²) _{3/2}	2	44.397	x-16	10 ^f	44.386	0.002	0.011
(1s ² 2s _{1/2} ² p _{1/2} ² p _{3/2} ³ d _{5/2}) _{1/2} → (1s ² 2s _{1/2} ² p _{1/2} ² p _{3/2} ²) _{1/2}	2	44.397	x-16	10 ^f	44.386	0.002	0.115
(1s ² 2s _{1/2} ² p _{3/2} ³ d _{5/2}) _{3/2} → (1s ² 2s _{1/2} ² p _{1/2} ² p _{3/2} ²) _{1/2}	1	44.501	x-16	10 ^f	44.386	0.002	0.115
(1s ² 2s _{1/2} ² p _{1/2} ² p _{3/2} ³ d _{5/2}) _{5/2} → (1s ² 2s _{1/2} ² p _{1/2} ² p _{3/2} ²) _{3/2}	1	44.506	x-16	10 ^f	44.386	0.002	0.120
(1s ² 2s _{1/2} ² p _{1/2} ² p _{3/2} ³ d _{5/2}) _{7/2} → (1s ² 2s _{1/2} ² p _{1/2} ² p _{3/2} ²) _{5/2}	1	44.851	x-17	4	44.565	0.006	0.286

TABLE 4—Continued

HULLAC Transition	HULLAC Intensity ^a	HULLAC		Measured			MEKAL		CHIANTI		
		λ (Å)	Feature	Measured Intensity ^a	λ (Å)	Standard Error	$\Delta\lambda^b$ (Å)	λ^c (Å)	$\Delta\lambda^d$ (Å)	λ^e (Å)	Comment
(1s ² s _{1/2} 2p _{1/2} 2p _{3/2} ² 3d _{5/2}) _{7/2} → (1s ² s _{1/2} 2p _{1/2} 2p _{3/2} ³) _{5/2}	1	45.536	x-18	8 ^f	45.287	0.004	0.249	Blend of two predicted lines, with viii-3
	1	45.578	x-18	8 ^f	45.287	0.004	0.291	Blend of two predicted lines, with viii-3
	2	46.263	x-19	7	45.980	0.004	0.283
	1	46.404	Blend of two predicted lines
	1	46.406	Blend of two predicted lines
	6	47.818	x-20	20	47.637	0.004	0.181	47.694	0.057
	3	47.969	x-21	15 ^f	47.809	0.009	0.160	47.793	-0.016	...	Blend of two predicted lines, with ix-8
	2	48.07	x-21	15 ^f	47.809	0.009	0.261	47.793	-0.016	...	Blend of two predicted lines, with ix-8
	1	48.336	x-22	9 ^f	48.158	0.002	0.178	Blend of two predicted lines, with ix-9
	2	48.379	x-22	9 ^f	48.158	0.002	0.221	Blend of two predicted lines, with ix-9
	2	49.354	49.127	0.003	0.227	Blend of two predicted lines, with ix-11
	1	49.385	49.127	0.003	0.258	Blend of two predicted lines, with ix-11
	1	49.506	x-23	5	49.326	0.004	0.180	Blend with ix-12
	1	50.401	x-24	2	50.398	0.006	0.003
	1	51.239	x-25	5 ^f	51.132	0.005	0.107	Blend of two predicted lines
	2	51.243	x-25	5 ^f	51.132	0.005	0.111	Blend of two predicted lines
	4	51.378	x-26	2	51.277	0.008	0.101
	2	51.544	x-27	3 ^f	51.434	0.014	0.110	Blend of two predicted lines
	1	51.64	x-27	3 ^f	51.434	0.014	0.206	Blend of two predicted lines
	1	53.218	Blend of two predicted lines, with viii
	2	54.302	Blend of two predicted lines, with viii
	2	54.489	Blend of two predicted lines, with vii
	1	54.596	Blend of two predicted lines, with vii
	1	54.816	Blend with viii
	1	54.934	x-28	1	54.765	0.017	0.169
	1	57.016	x-29	3 ^f	56.548	0.006	0.468	Blend of two predicted lines
	1	57.017	x-29	3 ^f	56.548	0.006	0.469	Blend of two predicted lines

^a Relative to strongest peak; scale 1–20.^b $\lambda_{\text{HULLAC}} - \lambda_{\text{EBIT}}$.^c Kaastra & Mewe (1993); Mewe et al. (1995b).^d $\lambda_{\text{MEKAL}} - \lambda_{\text{EBIT}}$.^e Dere et al. (1997, 2001).^f Combined intensity of blended feature.

TABLE 5
SUMMARY OF S XI EMISSION DATA

HULLAC Transition	HULLAC Intensity ^a	HULLAC		Measured		MEKAL			Comment
		λ (Å)	Feature	Measured Intensity ^a	λ (Å)	Standard Error	$\Delta\lambda^b$ (Å)	λ^c (Å)	
(1s ² 2s _{1/2} ² p _{3/2} ⁵ d _{5/2}) ₆ → (1s ² 2s _{1/2} ² p _{3/2}) ₄	1	28.404	xi-1	3	28.315	0.005	0.089
	<1	29.684	xi-2	2	29.549	0.003	0.135
	1	31.106	xi-3	6 ^e	31.050	0.003	0.056
	1	31.108	xi-3	6 ^e	31.050	0.003	0.058
	1	31.122	xi-3	6 ^e	31.050	0.003	0.072
	2	31.144	xi-3	6 ^e	31.050	0.003	0.094
	1	31.198	xi-3	6 ^e	31.050	0.003	0.148
	1	31.584	...	2	31.511	0.007	0.073
	1	34.652	...	3	34.623	0.009	0.029
	1	36.803
	2	37.723	xi-4	1 ^e	37.600	0.006	0.123	37.340	-0.260
	1	37.756	xi-4	1 ^e	37.600	0.006	0.156	37.340	-0.260
	1	37.833	xi-5	1 ^e	37.745	0.008	0.088	37.780	0.035
	1	37.873	xi-5	1 ^e	37.745	0.008	0.128	37.780	0.035
	2	37.910	xi-5	1 ^e	37.745	0.008	0.165	37.780	0.035
	3	37.937	xi-5	1 ^e	37.745	0.008	0.192	37.780	0.035
	1	38.731
	2	39.202	xi-6	2 ^e	39.081	0.005	0.121
	3	39.215	xi-6	2 ^e	39.081	0.005	0.134
	1	39.226	xi-7	2 ^e	39.081	0.005	0.145
	2	39.331	xi-7	20 ^e	39.287	0.002	0.044	39.240	-0.047
	7	39.342	xi-7	20 ^e	39.287	0.002	0.055	39.240	-0.047
	9	39.354	xi-7	20 ^e	39.287	0.002	0.067	39.240	-0.047
	13	39.388	xi-7	20 ^e	39.287	0.002	0.101	39.300	0.013
	2	39.416	xi-7	20 ^e	39.287	0.002	0.129	39.300	0.013
	20	39.427	xi-7	20 ^e	39.287	0.002	0.140	39.300	0.013
	8	39.735	xi-8	4 ^e	39.671	0.003	0.064
	1	39.824	xi-8	4 ^e	39.671	0.003	0.153
	1	40.359
	2	40.747
	1	40.773
	1	40.885
	1	41.108
	2	41.577
	2	41.661
	1	41.733
	1	42.193
	1	42.618
	1	43.164

TABLE 5—Continued

HULLAC Transition	HULLAC Intensity ^a	HULLAC λ (Å)	Measured Intensity ^a	Measured λ (Å)	Standard Error	MEKAL λ^c (Å)	MEKAL λ^d (Å)	Comment
		Feature						
(1s ² 2s _{1/2} ² 2p _{1/2} 3s _{1/2}) ₂ → (1s ² 2s _{1/2} ² 2p _{1/2}) ₀	1	43.264
(1s ² 2s _{1/2} ² 2p _{3/2} 3s _{1/2}) ₄ → (1s ² 2s _{1/2} ² 2p _{3/2}) ₄	3	43.304	xi-9	3 ^e	43.298	0.003	0.006	...
(1s ² 2s _{1/2} ² 2p _{1/2} 3s _{1/2}) ₀ → (1s ² 2s _{1/2} ² 2p _{1/2} 2p _{3/2}) ₂	1	43.406	xi-9	3 ^e	43.298	0.003	0.108	...
(1s ² 2s _{1/2} ² 2p _{1/2} 3s _{1/2}) ₂ → (1s ² 2s _{1/2} ² 2p _{3/2}) ₄	1	43.495	xi-9	3 ^e	43.298	0.003	0.197	...
(1s ² 2s _{1/2} ² 2p _{3/2} 3s _{1/2}) ₂ s → (1s ² 2s _{1/2} ² 2p _{1/2} 2p _{3/2}) ₄	1	44.112
(1s ² 2s _{1/2} ² 2p _{3/2} 3s _{1/2}) ₄ → (1s ² 2s _{1/2} ² 2p _{1/2} 2p _{3/2}) ₆	3	45.258	xi-10	2	45.008	0.006	0.250	...
(1s ² 2s _{1/2} ² 2p _{1/2} 2p _{3/2} 3s _{1/2}) ₂ → (1s ² 2s _{1/2} ² 2p _{1/2} 2p _{3/2}) ₄	2	45.387	xi-11	2 ^e	45.124	0.007	0.263	...
(1s ² 2s _{1/2} ² 2p _{1/2} 2p _{3/2} 3s _{1/2}) ₀ → (1s ² 2s _{1/2} ² 2p _{1/2} ² 2p _{3/2}) ₂	1	45.465	xi-11	2 ^e	45.124	0.007	0.341	...
(1s ² 2s _{1/2} ² 2p _{1/2} 2p _{3/2} 3s _{1/2}) ₄ → (1s ² 2s _{1/2} ² 2p _{1/2} ² 2p _{3/2}) ₄	1	46.333	Blend with x-19
(1s ² 2s _{1/2} ² 2p _{3/2} 3s _{1/2}) ₄ → (1s ² 2s _{1/2} ² 2p _{3/2}) ₄	2	46.577	Blend with ix-4
	6	47.809	0.009	...	Blend with x-21
(1s ² 2s _{1/2} ² 2p _{3/2} 3p _{1/2}) ₄ → (1s ² 2s _{1/2} ² 2p _{1/2} 2p _{3/2}) ₆	3	48.045	xi-12	3 ^e	48.158	0.002	-0.113	...
(1s ² 2s _{1/2} ² 2p _{3/2} 3p _{1/2}) ₂ → (1s ² 2s _{1/2} ² 2p _{1/2} 2p _{3/2}) ₄	1	48.108	xi-12	3 ^e	48.158	0.002	-0.050	...
(1s ² 2s _{1/2} ² 2p _{1/2} 3p _{1/2}) ₀ → (1s ² 2s _{1/2} ² 2p _{1/2} 2p _{3/2}) ₂	1	48.238	xi-12	3 ^e	48.158	0.002	0.080	...
	xi-13	3	49.714	0.007
(1s ² 2s _{1/2} ² 2p _{3/2} 3p _{3/2}) ₆ → (1s ² 2s _{1/2} ² 2p _{3/2}) ₄	1	49.991	xi-14	2	49.981	0.008	0.010	...
(1s ² 2s _{1/2} ² 2p _{3/2} 3p _{3/2}) ₄ → (1s ² 2s _{1/2} ² 2p _{1/2} 2p _{3/2}) ₄	1	52.004	Blend with viii

^a Relative to strongest peak; scale 1–20.^b $\lambda_{\text{HULLAC}} - \lambda_{\text{EBIT}}$.^c Kaastra & Mewe (1993); Mewe et al. (1995b).^d $\lambda_{\text{MEKAL}} - \lambda_{\text{EBIT}}$.^e Combined intensity of blended feature.

TABLE 6
SUMMARY OF S XII EMISSION DATA

HULLAC Transition	HULLAC			Measured			MEKAL		CHIANTI			Comment
	HULLAC Intensity ^a	λ (Å)	Feature	Measured Intensity ^a	λ (Å)	Standard Error	$\Delta\lambda^b$ (Å)	λ^c (Å)	$\Delta\lambda^d$ (Å)	λ^e (Å)	$\Delta\lambda^f$ (Å)	
(1s ² 2s _{1/2} ² 5d _{3/2}) _{3/2} → (1s ² s _{1/2} ² 2p _{1/2}) _{1/2}	1	25.645	xii-1	4 ^g	25.658	0.014	-0.013	Blend of two predicted lines
(1s ² 2s _{1/2} ² 5d _{5/2}) _{5/2} → (1s ² s _{1/2} ² 2p _{3/2}) _{3/2}	1	25.728	xii-1	4 ^g	25.658	0.014	0.070	Blend of two predicted lines
(1s ² 2s _{1/2} ² p _{3/2} ² 4p _{3/2}) _{5/2} → (1s ² 2s _{1/2} ² 2p _{3/2}) _{3/2}	1	26.907	27.800	Blend dominated by xiii-4
(1s ² 2s _{1/2} ² 4d _{3/2}) _{3/2} → (1s ² 2s _{1/2} ² 2p _{1/2}) _{1/2}	2	28.282	...	5 ^g	28.315	0.005	-0.033	Blend of two predicted lines; blend with xi
(1s ² 2s _{1/2} ² 4d _{5/2}) _{5/2} → (1s ² 2s _{1/2} ² 2p _{3/2}) _{3/2}	3	28.383	...	5 ^g	28.315	0.005	0.068	Blend of two predicted lines; blend with xi
(1s ² 2s _{1/2} ² p _{3/2} ³ p _{3/2}) _{5/2} → (1s ² 2s _{1/2} ² 2p _{3/2}) _{3/2}	1	32.871	xii-2	3 ^g	32.899	0.004	-0.028	Blend of two predicted lines
(1s ² 2s _{1/2} ² p _{3/2} ³ p _{1/2}) _{3/2} → (1s ² 2s _{1/2} ² 2p _{3/2}) _{3/2}	1	32.896	xii-2	3 ^g	32.899	0.004	-0.003	Blend of two predicted lines
(1s ² 2s _{1/2} ² p _{3/2} ³ p _{3/2}) _{1/2} → (1s ² 2s _{1/2} ² 2p _{3/2}) _{3/2}	1	34.350	Blend dominated by x-4
(1s ² 2s _{1/2} ² p _{1/2} ³ p _{3/2}) _{3/2} → (1s ² 2s _{1/2} ² 2p _{1/2}) _{1/2}	3	34.601	...	8 ^g	34.592	0.001	0.009	Blend of three predicted lines; blend with x-5
(1s ² 2s _{1/2} ² p _{3/2} ³ p _{3/2}) _{5/2} → (1s ² 2s _{1/2} ² 2p _{3/2}) _{3/2}	5	34.655	...	8 ^g	34.592	0.001	0.063	Blend of three predicted lines; blend with x-5
(1s ² 2s _{1/2} ² p _{1/2} ³ p _{3/2}) _{3/2} → (1s ² 2s _{1/2} ² 2p _{3/2}) _{3/2}	1	34.757	...	8 ^g	34.592	0.001	0.165	Blend of three predicted lines; blend with x-5
(1s ² 2s _{1/2} ² p _{1/2} ³ p _{3/2}) _{1/2} → (1s ² 2s _{1/2} ² 2p _{1/2}) _{1/2}	1	35.158	xii-3	3 ^g	35.221	0.006	-0.063	Blend of three predicted lines; blend with x-6
(1s ² 2s _{1/2} ² p _{1/2} ³ p _{3/2}) _{3/2} → (1s ² 2s _{1/2} ² 2p _{3/2}) _{3/2}	2	35.298	xii-3	3 ^g	35.221	0.006	0.077	Blend of three predicted lines; blend with x-6
(1s ² 2s _{1/2} ² p _{1/2} ³ p _{3/2}) _{3/2} → (1s ² 2s _{1/2} ² 2p _{3/2}) _{3/2}	1	35.369	xii-3	3 ^g	35.221	0.006	0.148	Blend of three predicted lines; blend with x-6
(1s ² 2s _{1/2} ² p _{3/2} ³ d _{5/2}) _{7/2} → (1s ² 2s _{1/2} ² p _{1/2} ² p _{3/2}) _{5/2}	1	35.932	xii-4	2	35.968	0.001	-0.036	Blend with x-9
(1s ² 2s _{1/2} ² p _{3/2} ³ d _{3/2}) _{5/2} → (1s ² 2s _{1/2} ² p _{1/2} ² p _{3/2}) _{3/2}	1	36.245	xii-5	13 ^g	36.397	0.003	-0.152	36.398	0.001	36.3980	0.001	Blend of two predicted lines
(1s ² 2s _{1/2} ² d _{3/2} ³ d _{3/2}) _{3/2} → (1s ² 2s _{1/2} ² p _{1/2}) _{1/2}	12	36.488	xii-5	13 ^g	36.397	0.003	0.091	36.398	0.001	36.3980	0.001	Blend of two predicted lines
(1s ² 2s _{1/2} ² d _{3/2} ³ d _{5/2}) _{5/2} → (1s ² 2s _{1/2} ² p _{3/2}) _{3/2}	20	36.649	xii-6	20 ^g	36.564	0.003	0.085	36.563	-0.001	36.5640	0.000	Blend of two predicted lines
(1s ² 2s _{1/2} ² d _{3/2} ³ d _{3/2}) _{3/2} → (1s ² 2s _{1/2} ² p _{3/2}) _{3/2}	2	36.662	xii-6	20 ^g	36.564	0.003	0.098	36.563	-0.001	36.5730	0.009	Blend of two predicted lines
(1s ² 2s _{1/2} ² p _{3/2} ³ d _{3/2}) _{3/2} → (1s ² 2s _{1/2} ² p _{1/2} ² p _{3/2}) _{1/2}	1	37.496	Blend dominated by xiii-10
(1s ² 2s _{1/2} ² p _{3/2} ³ d _{5/2}) _{5/2} → (1s ² 2s _{1/2} ² p _{3/2}) _{3/2}	1	37.558	Blend dominated by xiii-10
(1s ² 2s _{1/2} ² p _{3/2} ³ d _{3/2}) _{7/2} → (1s ² 2s _{1/2} ² p _{1/2} ² p _{3/2}) _{5/2}	4	37.722	37.715	...	Blend with xi-5
(1s ² 2s _{1/2} ² p _{1/2} ³ d _{5/2}) _{5/2} → (1s ² 2s _{1/2} ² p _{1/2} ² p _{3/2}) _{3/2}	3	37.836	Blend with xi-5
(1s ² 2s _{1/2} ² p _{1/2} ³ d _{1/2}) _{3/2} → (1s ² 2s _{1/2} ² p _{1/2} ² p _{3/2}) _{3/2}	1	38.546	xii-7	2	38.326	0.008	0.220
(1s ² 2s _{1/2} ² p _{3/2} ³ d _{5/2}) _{1/2} → (1s ² 2s _{1/2} ² p _{3/2}) _{1/2}	1	39.026	xii-8	5 ^g	38.900	0.005	0.126	Blend of two predicted lines
(1s ² 2s _{1/2} ² p _{3/2} ³ d _{5/2}) _{3/2} → (1s ² 2s _{1/2} ² p _{3/2}) _{1/2}	2	39.096	xii-8	5 ^g	38.900	0.005	0.196	Blend of two predicted lines
(1s ² 2s _{1/2} ² s _{1/2} ³ s _{1/2}) _{1/2} → (1s ² 2s _{1/2} ² p _{1/2}) _{1/2}	1	39.252	Blend dominated by xi-7
(1s ² 2s _{1/2} ² s _{1/2} ³ s _{1/2}) _{1/2} → (1s ² 2s _{1/2} ² p _{3/2}) _{3/2}	2	39.452	Blend dominated by xi-7
(1s ² 2s _{1/2} ² p _{3/2} ³ s _{1/2}) _{3/2} → (1s ² 2s _{1/2} ² p _{1/2} ² p _{3/2}) _{5/2}	4	40.755	xii-9	6	40.543	0.008	0.212
(1s ² 2s _{1/2} ² p _{1/2} ³ s _{1/2}) _{1/2} → (1s ² 2s _{1/2} ² p _{1/2} ² p _{3/2}) _{5/2}	2	40.898
(1s ² 2s _{1/2} ² p _{1/2} ³ s _{1/2}) _{3/2} → (1s ² 2s _{1/2} ² p _{1/2} ² p _{3/2}) _{1/2}	1	42.378	Carbon edge
(1s ² 2s _{1/2} ² p _{1/2} ³ s _{1/2}) _{1/2} → (1s ² 2s _{1/2} ² p _{1/2} ² p _{3/2}) _{1/2}	1	42.538	Carbon edge
(1s ² 2s _{1/2} ² p _{3/2} ³ d _{5/2}) _{3/2} → (1s ² 2s _{1/2} ² p _{1/2} ² p _{3/2}) _{5/2}	3	43.574	Blend dominated by x-12
(1s ² 2s _{1/2} ² p _{1/2}) _{1/2} → (1s ² 2s _{1/2} ² p _{1/2} ² p _{3/2}) _{3/2}	2	43.635	Blend dominated by x-12

^a Relative to strongest peak, scale 1–20.

^b $\lambda_{\text{HULLAC}} - \lambda_{\text{EBIT}}$.

^c Kaastra & Mewe (1993); Mewe et al. (1995b).

^d $\lambda_{\text{MEKAL}} - \lambda_{\text{EBIT}}$.

^e Dere et al. (1997, 2001).

^f $\lambda_{\text{CHIANTI}} - \lambda_{\text{EBIT}}$.

^g Combined intensity of blended feature.

TABLE 7
SUMMARY OF S XIII EMISSION DATA

HULLAC Transition	HULLAC Intensity ^a	HULLAC λ (Å)	Measured Feature	Measured Intensity ^a	Measured λ (Å)	Standard Error	MEKAL λ^c (Å)	CHIANTI λ^e (Å)	$\Delta\lambda^d$	$\Delta\lambda^f$	Comment
(1s ² 2s _{1/2} 5p _{3/2}) ₂ → (1s ² 2s _{1/2}) ₀	1	22.213	xiii-1	4	22.204	0.010	0.009
.....	23.100
(1s ² 2s _{1/2} 5d _{5/2}) ₄ → (1s ² 2s _{1/2} 2p _{3/2}) ₂	1	24.331	xiii-2	8	24.415	0.008	-0.084
(1s ² 2s _{1/2} 4p _{3/2}) ₂ → (1s ² 2s _{1/2}) ₀	4	24.589	xiii-3	13	24.590	0.003	-0.001
.....	26.400
(1s ² 2s _{1/2} 4d _{5/2}) ₄ → (1s ² 2s _{1/2} 2p _{3/2}) ₂	3	27.089	xiii-4	3	26.973	0.005	0.116
(1s ² 2s _{1/2} 4s _{1/2}) ₀ → (1s ² 2s _{1/2} 2p _{3/2}) ₂	1	27.514	xiii-5	3	27.405	0.005	0.109
(1s ² 2s _{1/2} 3p _{3/2}) ₂ → (1s ² 2s _{1/2}) ₀	4	32.201	xiii-6	20 ^g	32.238	0.003	-0.037	32.236	-0.002	32.1910	-0.047
.....
(1s ² 2s _{1/2} 3p _{1/2}) ₂ → (1s ² 2s _{1/2}) ₀	19	32.247	xiii-6	20 ^g	32.238	0.003	0.009	32.236	-0.002	32.2420	0.004
(1s ² 2s _{1/2} 3d _{3/2}) ₄ → (1s ² 2s _{1/2} 2p _{1/2}) ₂	1	33.855	xiii-7	5	33.821	0.002	0.034	33.843	0.023	...	Shoulder of xiii-8
(1s ² 2s _{1/2} 3d _{5/2}) ₆ → (1s ² 2s _{1/2} 2p _{3/2}) ₄	2	33.955	xiii-8	13	33.942	0.003	0.013	33.945	0.003	33.9510	0.009
(1s ² 2s _{1/2} 3d _{5/2}) ₄ → (1s ² 2s _{1/2} 2p _{3/2}) ₂	20	35.849	xiii-9	20	35.669	0.003	0.180	35.614	-0.055	35.6670	-0.002
.....	xiii-9	20	35.669	0.003	...	35.665	-0.004
(1s ² 2s _{1/2} 3d _{5/2}) ₂ → (1s ² 2p _{3/2}) ₀	2	36.698	Blend with xii
(1s ² 2p _{3/2} 3s _{1/2}) ₂ → (1s ² 2p _{1/2} 2p _{3/2}) ₄	1	36.923
(1s ² 2s _{1/2} 3s _{1/2}) ₀ → (1s ² 2s _{1/2} 2p _{3/2}) ₂	10	37.844	xiii-10	19	37.609	0.003	0.235	37.600	-0.009	37.598	-0.011
(1s ² 2s _{1/2} 3p _{3/2}) ₄ → (1s ² 2p _{1/2}) ₄	1	38.943	Blend with xii-8

^a Relative to strongest peak; scale 1–20.

^b $\lambda_{\text{HULLAC}} - \lambda_{\text{EBIT}}$.

^c Kaastra & Mewe (1993); Mewe et al. (1995b).

^d $\lambda_{\text{MEKAL}} - \lambda_{\text{EBIT}}$.

^e Dere et al. (1997, 2001).

^f $\lambda_{\text{CHIANTI}} - \lambda_{\text{EBIT}}$.

^g Combined intensity of blended feature.

TABLE 8
SUMMARY OF S XIV EMISSION DATA

HULLAC Transition	HULLAC Intensity ^a	HULLAC λ (Å)	HULLAC Feature	Measured Intensity ^a	Measured λ (Å)	Standard Error	MEKAL λ ^e (Å)	MEKAL $\Delta\lambda$ ^b (Å)	CHIANTI λ ^e (Å)	CHIANTI $\Delta\lambda$ ^f (Å)	Comment
$(1s^2 5d_{5/2})_{5/2} \rightarrow (1s^2 2p_{3/2})_{3/2}$	1	21.740	xiv-1	13	21.613	0.008	0.127
$(1s^2 4p_{3/2})_{3/2} \rightarrow (1s^2 2s_{1/2})_{1/2}$	3	23.010	xiv-2	17 ^g	23.020	0.007	-0.010	23.050	0.030	23.005	-0.015 Blend of two predicted lines
$(1s^2 4p_{1/2})_{1/2} \rightarrow (1s^2 2s_{1/2})_{1/2}$	1	23.020	xiv-2	17 ^g	23.020	0.007	0.000	23.050	0.030	23.015	-0.005 Blend of two predicted lines
$(1s^2 4d_{3/2})_{3/2} \rightarrow (1s^2 2p_{1/2})_{1/2}$	1	24.214	xiv-3	20 ^g	24.257	0.006	-0.043	24.200	-0.057	24.200	-0.057 Blend of two predicted lines
$(1s^2 4d_{5/2})_{5/2} \rightarrow (1s^2 2p_{3/2})_{3/2}$	2	24.298	xiv-3	20 ^g	24.257	0.006	0.041	24.200	-0.057	24.285	0.028 Blend of two predicted lines
1057											
$1s^2 4s_{1/2})_{1/2} \rightarrow (1s^2 2p_{3/2})_{3/2}$	1	24.521	24.415	0.008	24.418	0.003 ...
$(1s^2 3p_{3/2})_{3/2} \rightarrow (1s^2 2s_{1/2})_{1/2}$	20	30.436	xiv-4	18 ^g	30.447	0.005	-0.011	30.423	-0.024	30.427	-0.020 Blend of two predicted lines
$(1s^2 3p_{1/2})_{1/2} \rightarrow (1s^2 2s_{1/2})_{1/2}$	10	30.477	xiv-4	18 ^g	30.447	0.005	0.030	30.423	-0.024	30.469	0.022 Blend of two predicted lines
$(1s^2 3d_{3/2})_{3/2} \rightarrow (1s^2 2p_{1/2})_{1/2}$	9	32.437	xiv-5	11	32.415	0.006	0.022	32.430	0.015	32.416	0.001 ...
$1s^2 3d_{5/2})_{5/2} \rightarrow (1s^2 2p_{3/2})_{3/2}$	17	32.58	xiv-6	15 ^g	32.559	0.003	0.021	32.554	-0.005	32.560	0.001 Blend of two predicted lines
$1s^2 3d_{3/2})_{3/2} \rightarrow (1s^2 2p_{3/2})_{3/2}$	2	32.594	xiv-6	15 ^g	32.559	0.003	0.035	32.554	-0.005	32.575	0.016 Blend of two predicted lines
$1s^2 3s_{1/2})_{1/2} \rightarrow (1s^2 2p_{1/2})_{1/2}$	5	33.404	xiv-7	2	33.383	0.008	0.021	33.259	-0.124	33.381	-0.002 ...
$1s^2 3s_{1/2})_{1/2} \rightarrow (1s^2 2p_{3/2})_{3/2}$	9	33.572	xiv-8	4	33.560	0.006	0.012	33.425	-0.135	33.549	-0.011 ...

^a Relative to strongest peak; scale 1–20.

^b $\lambda_{\text{HULLAC}} - \lambda_{\text{EBIT}}$.

^c Kaastra & Mewe (1993); Mewe et al. (1995b).

^d $\lambda_{\text{MEKAL}} - \lambda_{\text{EBIT}}$.

^e Dere et al. (1997, 2001).

^f $\lambda_{\text{CHIANTI}} - \lambda_{\text{EBIT}}$.

^g Combined intensity of blended feature.

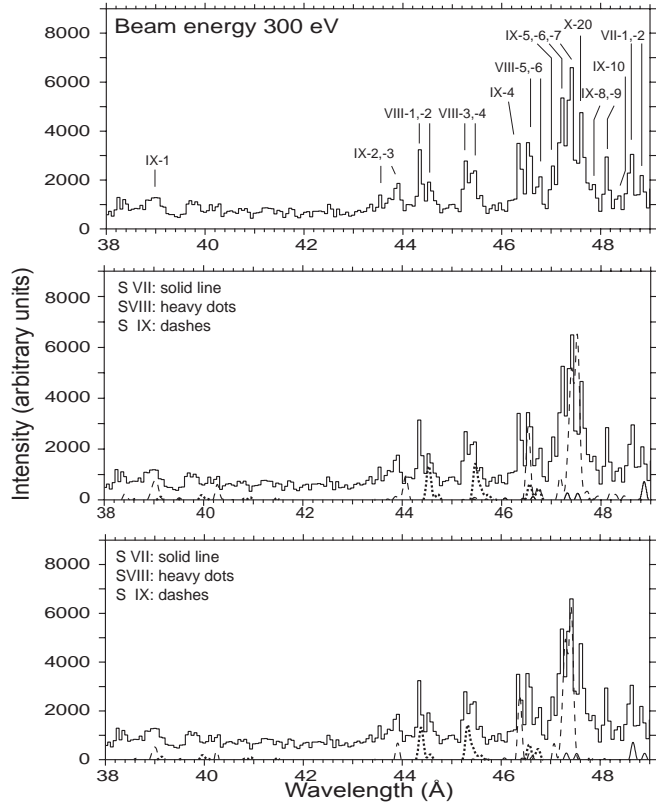


Fig. 2.—Comparison of EBIT-II spectrum and synthetic spectra constructed with HULLAC calculations. Beam energy is 300 eV, wavelength range 38–49 Å. Top: EBIT-II spectrum. Lack of lines near 42 Å is due to the carbon edge. Middle: EBIT-II data overlaid with synthetic HULLAC spectra, intensity adjusted for the detector response and normalized to the strongest measured peak in each charge state. Note that for some ions, the strongest peak is not in range of the graph. For example, the peak to which S viii lines are normalized is found in Fig. 3. Bottom: EBIT-II overlaid with HULLAC, in which each line has been adjusted to match the experimentally determined position. This is the “best attempt” to reconcile theory with experiment.

Our spectra also contain a line not predicted by calculations. This line corresponds to the $(1s^2 2s_{1/2}^2 2p_{1/2} 2p_{3/2}^4 3s_{1/2})_0 \rightarrow (1s^2 2s_{1/2}^2 2p_{1/2}^2 2p_{3/2}^4)_0$ transition in S vii and is labeled S vii-9 in the figures and in Table 1. This transition is strictly forbidden by selection rules. However, it becomes possible if the ion is embedded in a magnetic field, as described by Beiersdorfer et al. (2003). The S vii line is a spectral diagnostic of magnetic field strength and increases in strength relative to the 3F line (S vii-8) as the magnetic field is increased. The magnetic field in EBIT-I and EBIT-II is 30 kG, and it is sufficient to produce the line even in the presence of collisions.

5. COMPARISON WITH PROCYON

Raassen et al. (2002; their Tables 1 and 2) identified a number of possible lines of S vii through S xiii in the region 20–75 Å in a spectrum of Procyon taken with the *Chandra* Low Energy Transmission Grating Spectrometer (LETGS). They listed 15 lines from *Chandra* for which sulfur was given as a possible identification in either MEKAL (Kaastra & Mewe 1993; Mewe et al. 1995), Kelly (1987), or Doschek & Cowan (1984). In some cases, sulfur was just one of several identification possibilities. We compared EBIT-II spectra to the *Chandra* data by overlaying the two. This allows a quick visual confirmation of the presence of each charge state, since not only must there be lines in the same locations, but they also must match in relative intensity. From this we identify the presence of S vii through S xi.

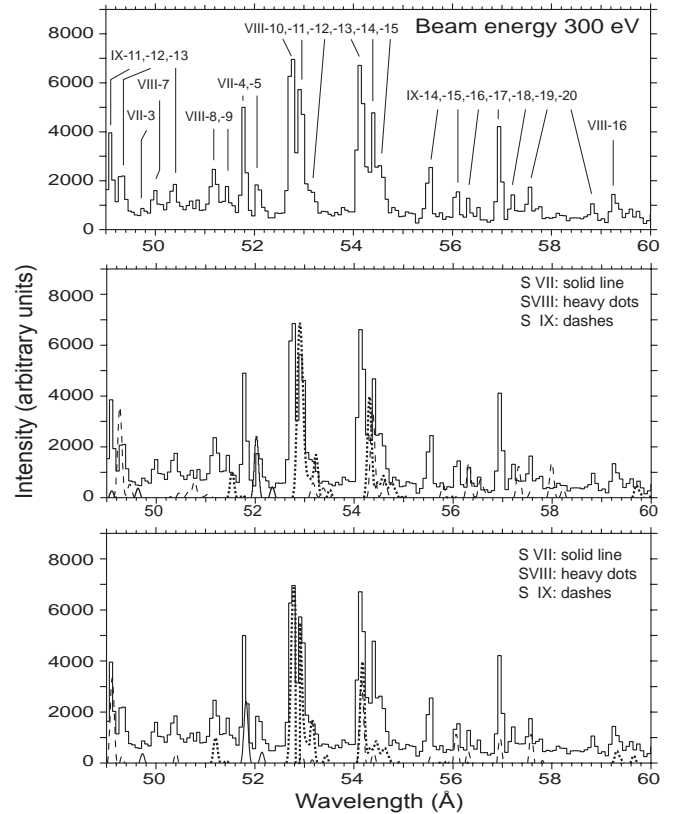


Fig. 3.—Comparison of EBIT-II spectrum and synthetic spectra constructed with HULLAC calculations. Beam energy is 300 eV, wavelength range 49–60 Å. Notations are the same as for Fig. 2.

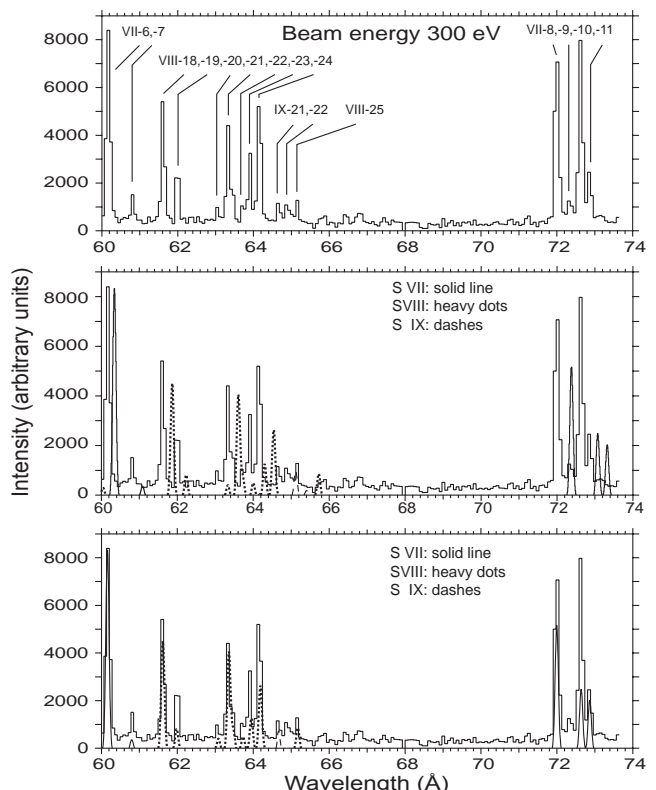


Fig. 4.—Comparison of EBIT-II spectrum and synthetic spectra constructed with HULLAC calculations. Beam energy is 300 eV, wavelength range 60–74 Å. Notations are the same as for Fig. 2.

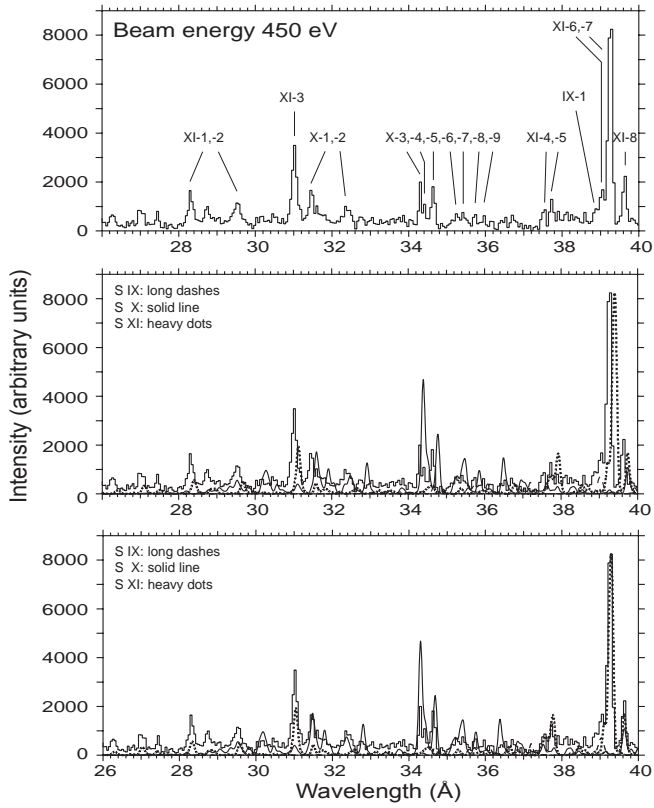


FIG. 5.—Comparison of EBIT-II spectrum and synthetic spectra constructed with HULLAC calculations. Beam energy is 450 eV, wavelength range 26–40 Å. Notations are the same as for Fig. 2.

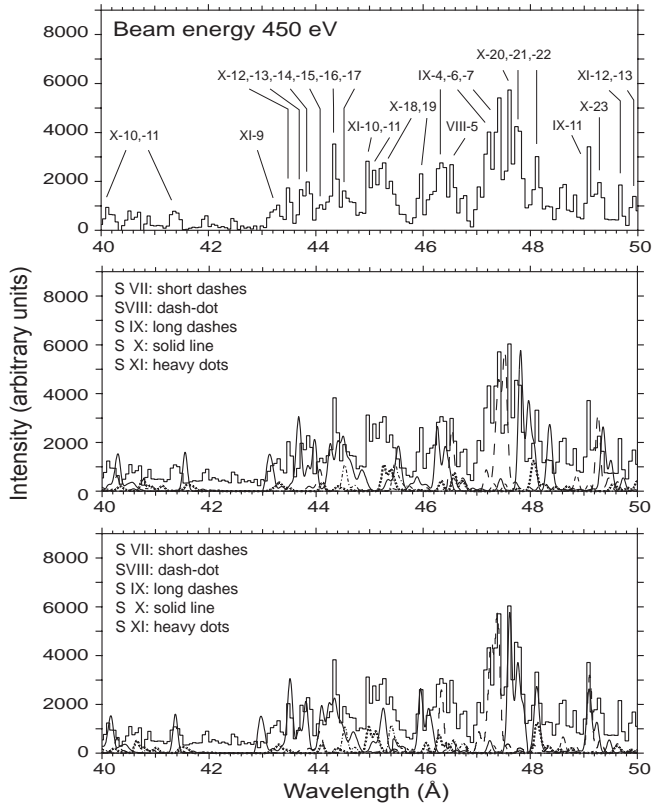


FIG. 6.—Comparison of EBIT-II spectrum and synthetic spectra constructed with HULLAC calculations. Beam energy is 450 eV, wavelength range 40–50 Å. Notations are the same as for Fig. 2.

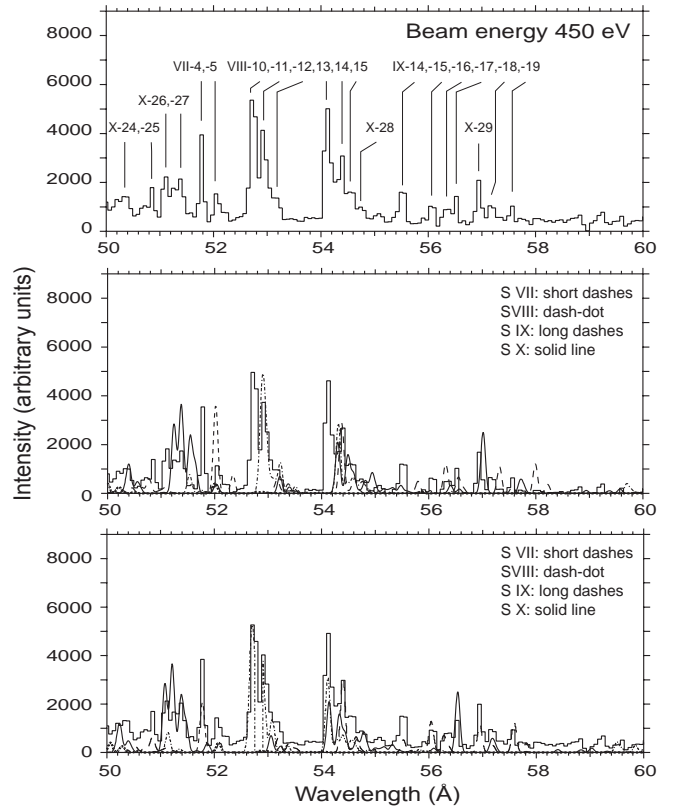


FIG. 7.—Comparison of EBIT-II spectrum and synthetic spectra constructed with HULLAC calculations. Beam energy is 450 eV, wavelength range 50–60 Å. Notations are the same as for Fig. 2.

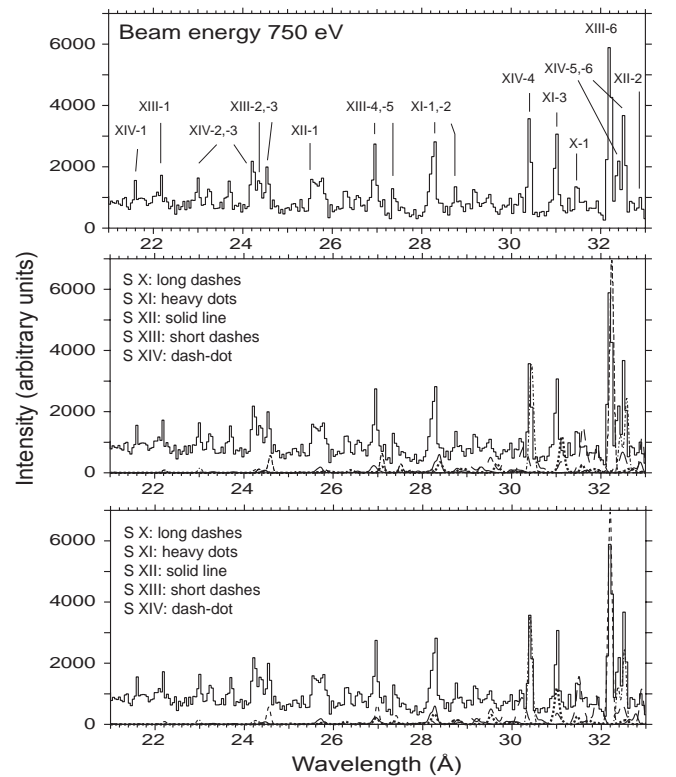


FIG. 8.—Comparison of EBIT-II spectrum and synthetic spectra constructed with HULLAC calculations. Beam energy is 750 eV, wavelength range 21–33 Å. Notations are the same as for Fig. 2.

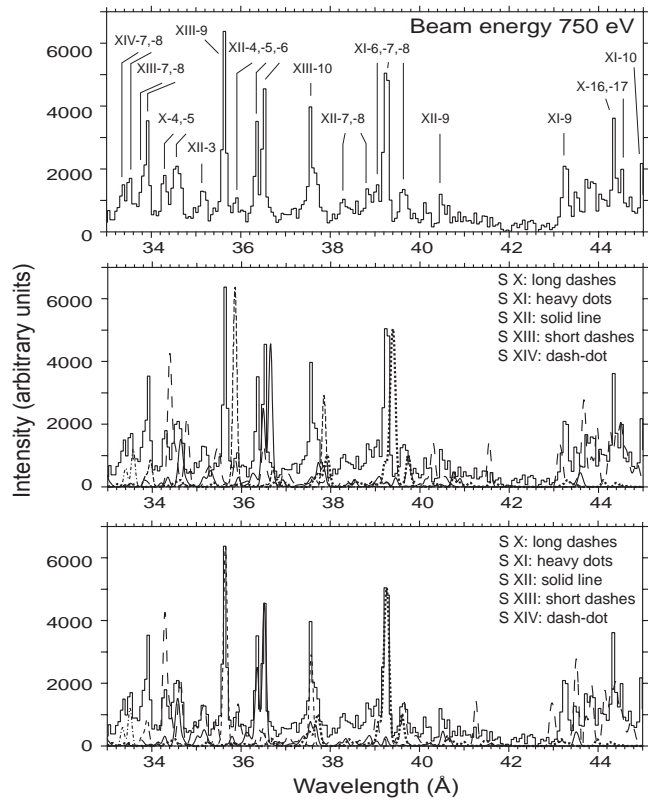


FIG. 9.—Comparison of EBIT-II spectrum and synthetic spectra constructed with HULLAC calculations. Beam energy is 750 eV, wavelength range 33–45 Å. Notations are the same as for Fig. 2.

The presence of S XII and S XIII is doubtful; if they are present they are in very small amounts. We found no evidence of S XIV. In Figure 10 we show overlays of a spectrum from the *Chandra* LETGS with spectra from EBIT-II for S VII, S VIII, and S IX–S X. The *Chandra* spectrum (obsID = 01461, 70.4 ks) was taken directly from Raassen et al. (2002), to which we direct the reader for details of processing the data. The *Chandra* spectra have a higher resolution than the EBIT-II data shown here, but the line clusters are evident. In some cases, blends with other elements in Procyon make the matches less obvious; e.g., the S IX and S X lines at 49.3 Å (Fig. 10c) blend with Ar IX in the *Chandra* spectrum. We have acquired a new spectrometer with resolution comparable to that of *Chandra* (Beiersdorfer et al. 2004), with which we intend to take further measurements, particularly of S X, whose strongest lines lie in the region of the

TABLE 9
COMPARISON OF EBIT-II DATA WITH MAJOR DATABASES

Charge State	EBIT-II	MEKAL ^a	CHIANTI ^b
S VII	10	9	0
S VIII	25	6	0
S IX	22	3	0
S X	29	5	1
S XI	14	4	0
S XII	9	3	4
S XIII	10	8	5
S XIV	8	9	13

NOTES.—Columns list the number of lines for each charge state. Data are for the region 20–75 Å.

^a Kaastra & Mewe (1993); Mewe et al. (1995b).

^b Dere et al. (1997, 2001).

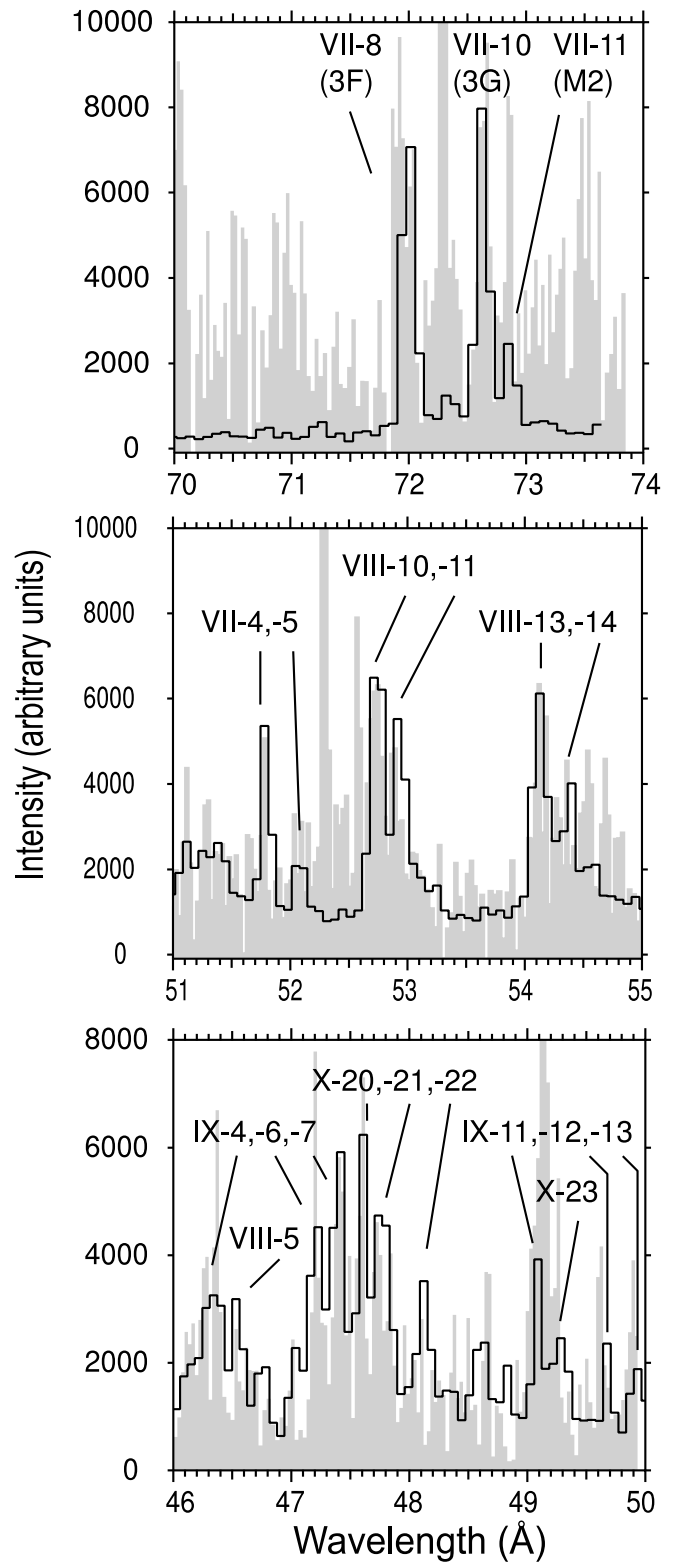


FIG. 10.—Comparison of EBIT-II sulfur spectra (black line) with *Chandra* spectrum of Procyon (gray filled area). Strong EBIT-II lines are labeled as in the figures and tables. Top: Taken at beam energy of 300 eV, highlighting S VII. Middle: Taken at beam energy of 400 eV, highlighting S VIII. Bottom: Taken at beam energy of 510 eV, highlighting S IX and S X.

carbon edge and are thus not seen in the present spectra because of a carbon film on the detector.

The spectrum of S VII merits further discussion, as there is a notable difference between our measurements and *Chandra* observations. The $3s \rightarrow 2p$ line at 72.9 Å, labeled VII-10 in Table 1 (commonly referred to as 3G), is much stronger compared to its companion at 72.7 Å, labeled VII-11 (commonly referred to as 3H or M2), in the *Chandra* spectrum than in our measurements. The latter line is density dependent, and its larger size in Procyon is indicative of a lower density than the density of $\sim 10^{11} \text{ cm}^{-3}$ in our electron beam ion trap. One of the strongest S VII lines, the $3d \rightarrow 2p$ line at 60.2 Å (labeled VII-6 in Fig. 4 and Table 1, commonly referred to as 3C), is not visible in the *Chandra* spectrum published by Raassen et al. (2002), nor is it listed in their Table 2. This line is located on a chip gap in the +1 order and close to the chip gap in the -1 order. As it is near the chip gap, it might be affected by a reduced instrumental response function (R. Mewe 2003, private communication). We did find it to be visible, albeit rather weakly, in the -1 order of ObsID 1461, and even more weakly in ObsID 63, which shows the need to analyze multiple observations for the most accurate results.

6. CONCLUSIONS

Our work here illustrates the need for careful laboratory measurements of isolated ions and elements in order to accurately identify and correlate emission lines with theoretical predictions. Most strong lines and some weaker lines can be identified with some confidence, as long as not too many different charge states are present. However, the density of weak lines prevents un-

equivocal identification of all lines, given the resolving power of our present instrumentation and the accuracy of the calculations. Despite these limitations, we find the laboratory spectra to be a useful aid for the analysis of spectra from *Chandra*. We also compared our results with published spectra from the DXS mission (Sanders et al. 2001), but none of the sulfur lines we found can account for the unexplained feature near 67.4 Å seen in DXS. We are concerned with overreliance on published databases that are compilations of theoretical calculations. As we have demonstrated, even the best atomic modeling codes must rely on laboratory measurements to get the correct numbers. We believe the measurements presented here are a significant step toward completely cataloging astrophysically relevant EUV and soft X-ray ions. Future measurements using our new ultra-high-resolution grating spectrometer will enable us to make more precise measurements and should allow us to extend these measurements to ever weaker emission lines.

We thank the late Rolf Mewe for assistance with interpreting the LETGS spectrum, Ming Feng Gu for providing us with spectra for ObsID 63 and ObsID 1461, and Randall Smith for many useful comments to help improve this paper. This work was supported by NASA Space Astrophysics Research and Analysis grant W-19,878 and was performed under the auspices of the Department of Energy by the University of California Lawrence Livermore National Laboratory under contract W-7405-ENG-48. E. B. was supported by grant 2002111 from the United States-Israel Binational Science Foundation (BSF), Jerusalem, Israel.

REFERENCES

- Bar-Shalom, A., Klapisch, M., & Oreg, J. 2001, *J. Quant. Spectrosc. Radiat. Transfer*, 71, 169
- Behar, E., Cottam, J., & Kahn, S. M. 2001, *ApJ*, 548, 966
- Beiersdorfer, P., Crespo López-Urrutia, J. R., Springer, P., Utter, S. B., & Wong, K. L. 1999a, *Rev. Sci. Instrum.*, 70, 276
- Beiersdorfer, P., Lepson, J. K., Brown, G. V., Utter, S. B., Kahn, S. M., Liedahl, D. A., & Mauche, C. W. 1999b, *ApJ*, 519, L185
- Beiersdorfer, P., Magee, E., Träbert, E., Chen, H., Lepson, J. K., Gu, M.-F., & Schmidt, M. 2004, *Rev. Sci. Instrum.*, 75, 3723
- Beiersdorfer, P., Scofield, J. H., & Osterheld, A. L. 2003, *Phys. Rev. Lett.*, 90, 235003
- Brinkmann, A. C., et al. 2000, *ApJ*, 530, L111
- Brown, G. V., Beiersdorfer, P., Liedahl, D. A., Widmann, K., Kah, S. M., & Clothiaux, E. J. 2002, *ApJS*, 140, 589
- Dere, K. P., Landi, E., Mason, H. E., Monsignori Fossi, B., & Young, P. R. 1997, *A&AS*, 125, 149
- Dere, K. P., Landi, E., Young, P. R., & Del Zanna, G. 2001, *ApJS*, 134, 331
- Doschek, G. A., & Cowan, R. D. 1984, *ApJS*, 56, 67
- Gu, M.-F. 2005, *ApJS*, 156, 105
- Harada, T., & Kita, T. 1980, *Appl. Opt.*, 19, 3987
- Kaastra, J. S., & Mewe, R. 1993, *Legacy*, 3, 6
- Kelly, R. L. 1987, *Atomic and Ionic Spectrum Lines below 2000 Angstroms: Hydrogen through Krypton* (New York: AIP)
- Klapisch, M., Schwob, J. L., Fraenkel, B. S., & Oreg, J. 1977, *J. Opt. Soc. Am.*, 67, 148
- Lepson, J. K., Beiersdorfer, P., Behar, E., & Kahn, S. M. 2003, *ApJ*, 590, 604
- Lepson, J. K., Beiersdorfer, P., Brown, G. V., Chen, H., Gullikson, E. M., Schneider, M. B., Utter, S. B., & Wong, K. L. 2001, Univ. California Lawrence Livermore Natl. Lab. Rep. UCRL-ID-142264, <http://www.llnl.gov/tid/lof/documents/pdf/245194.pdf>
- Lepson, J. K., et al. 2002, *ApJ*, 578, 648
- Mewe, R., Kaastra, J. S., & Liedahl, D. A. 1995a, *Legacy*, 6, 16
- Mewe, R., Kaastra, J. S., Schrijver, C. J., van den Oord, G. H. J., & Alkemade, F. J. M. 1995b, *A&A*, 296, 477
- Nakano, N., Kuroda, H., Kita, T., & Harada, T. 1984, *Appl. Opt.*, 23, 2386
- Raassen, A. J. J., Mewe, R., Audard, M., Güdel, M., Kaastra, J. S., van der Meer, R. L. J., Foley, C. R., & Ness, J.-U. 2002, *A&A*, 389, 228
- Sanders, W. T., Edgar, R. J., Kraushaar, W. L., McCammon, D., & Morgenthaler, J. P. 2001, *ApJ*, 554, 694
- Schmitt, J. H. M. M., Drake, J. J., & Stern, R. A. 1996, *ApJ*, 465, L51
- Utter, S. B., Brown, G. V., Beiersdorfer, P., Clothiaux, E. G., & Podder, N. K. 1999, *Rev. Sci. Instrum.*, 70, 284